Immune profiling, microbiome, metabolomics, and gut physiology of a 1-year controlled human hookworm infection

Authors: Francesco Vacca[1], Brittany Lavender[1], Sophia-Louise Noble[1], Alissa Cait[1], Kate Maclean[1], John Mamum[1], Bibek Yumnam[1], Tama Te Kawa[1], Thomas C Mules[1], Laura Ferrer-Font[1], Jeffry S. Tang[1], Olivier Gasser[1], Graham Le Gros[1], Mali Camberis[1*#], Stephen Inns[2#]

Affiliations:

[1]Malaghan Institute of Medical Research; Wellington 6012, New Zealand.

[2]Department of Medicine, Otago University, Wellington 6242, New Zealand.

[*]Corresponding author: mcamberis@malaghan.org.nz

[#]Co-last authors

One Sentence Summary: Controlled human hookworm infection changes immune-linked metabolic pathways

Abstract:

The observation that experimental helminth infection can be associated with immunomodulation and suppression of inflammatory diseases at distal tissue sites, has been used as rationale for trialing helminths such as *Necator americanus* for the treatment of inflammatory disorders in humans. However, the lack of sufficient knowledge of the immunological interplay between human host and parasite in a controlled infection setting limits ongoing clinical intervention studies. In this one-year longitudinal study, healthy volunteers were recruited and infected with *N. americanus*. Changes in immune responses, microbiome, plasma metabolome and gut physiology were examined over the course of the one-year period. All participants were successfully infected as confirmed by detectable eggs in the feces and adult worms visualized in the intestine. In general, individual variation in immune cells, serum cytokines, fecal microbiome and plasma metabolites were greater than changes induced by the infection. Nevertheless, eosinophils, serum IL-5, and fecal eosinophil degranulation markers transiently increased in the acute phase of infection. In addition, while we observed stability in microbial community composition through the course of infection, we found a difference in the microbial community composition of participants with moderate gastrointestinal symptoms. No significant changes were observed in gut physiology measured using Smartpill^{TM}, except for a decrease in small bowel pH. Untargeted plasma metabolomics analysis of participant plasma over the course of infection revealed enrichment in tryptophan metabolism following infection which was associated with increased CTLA-4 expression on regulatory T cells (T_{REGS}), CRTH2^{+} T helper 2 cells (T_H2) and CCR6^{+} T helper 9 cells (T_H9). In conclusion, hookworm infection is well tolerated and represents an innovative platform for investigating immunomodulatory properties of hookworm infection in a therapeutic clinical setting.

Main Text:

INTRODUCTION

Necator americanus (*Na*) is a species of hookworm that infects many millions of people in subtropical areas of the world*(1–3)*. The parasite/host relationship that has evolved between *Na* and humans has been formed over several millions of years *(4)* and features a immunological accommodation by the human host of the adult worm for up to ten years. The long term nature of hookworm infection of humans implies that compromising host survival is not in the best interests of the hookworm, and it has been hypothesized that chronic *Na* infection can confer beneficial immunomodulatory effects on the human host *(5, 6)*. This and the observation that inflammatory diseases have become increasingly prevalent in regions where hookworm has been eradicated, has led researchers to investigate potential positive effects of hookworm infection*(6, 7)*. Pioneering studies carried out in Africa and South America have observed reductions in atopic sensitization in those individuals carrying hookworm *(8–10)*. Furthermore, populations from hookworm endemic areas present with a signature regulatory T cell (T_{REG}) phenotype that is not found in non-infected populations. Anti-helminth treatment decreased this regulatory T cell signature, providing further evidence for helminths ability to regulate the immune system of their human host*(11)*. Clinical studies aimed at defining the immunoregulatory effects of hookworm infections in healthy volunteers demonstrate transient production of type 2 cytokines and acute increases in eosinophilia, that return to background levels as the adult hookworm establishes itself in the small intestine, indicating an active immune suppression of the human host by the adult parasites*(12–15)*. Further clinical studies have determined the safety profiles of *Na* infection, immune and immunoregulatory responses, for vaccine development, and patients suffering from IBD, celiac disease and multiple sclerosis *(12, 16–24)*. We sought to extend these controlled hookworm infection studies, by investigating the effect of the different phases of a controlled

hookworm infection on the immune regulatory networks, microbiome, metabolome, and gut physiology of healthy individuals. Participants were followed for one year and 30 *Na* L3 infective larvae were used to establish stable infection. The potency of infection was determined by collecting stool samples at multiple time points for egg counts. All participants were successfully infected with *Na* and a transient increase in eosinophils and markers associated with eosinophilic inflammation was observed. No other serum cytokines or immune cells were perturbated by the hookworm infection. While microbial communities remained stable during the infection, participants who experienced moderate gastrointestinal symptomology had a significantly different microbiome from those who experienced mild or absent symptoms. We also observed a decrease in small intestine pH. Furthermore, hookworm infection-induced changes were observed for tryptophan metabolism and expression of CTLA-4 in T_H2, T_{REGS} and T_H9 cells. With this study we have been able to gain a comprehensive picture of the range of human immunological, metabolic, and physiological responses induced by *Na* infection in healthy volunteers. This data set provides a platform for considering the use of controlled hookworm infection for the treatment of inflammatory diseases and vaccine development in humans.

RESULTS

Necator americanus infection induces tissue-specific symptoms

In this study 13 individuals with no history of allergies, auto-immune disease or inflammatory gut conditions completed the study (Fig1A and Table 1). We inoculated participants with 30 infective L_3 (iL_3) and followed host immune responses, microbiome, and gut physiology (Fig. 1B) during the acute and chronic phase of infection (Fig. 2A). Participants monitored symptoms they experienced for the first 12 weeks of infection (e.g., dermatological reaction, respiratory and gastrointestinal symptoms). Skin reactions (e.g., rash and itchiness) were observed mainly during the first weeks (Fig. 2B). Similarly, minor respiratory symptoms (e.g., cough, sneezing or sore throat) were observed by one participant during the first weeks (Fig. 2B), consistent with the lung phase of the parasite infection cycle. The majority of gastrointestinal (GI) symptoms were reported at 5- and 6-weeks post-infection, indicating the parasite reaching the gut lumen (Fig. 2B). No severe reactions were reported, indicating good tolerability of *Na* infection. With a view to enabling long-term storage and batched supply of hookworm larvae, cryopreservation was performed using methods previously described*(25)* and 4 of the 12 participants of this study received cryopreserved larvae which had been reanimated. Eggs were detectable in fecal samples from week 8 of infection onwards in all participants with similar egg production kinetics observed for those participants that received either cryopreserved or fresh larvae (Fig. 2C). Transient GI symptoms preceded egg detection in the feces (Fig. S1A) and two participants that chose to retain the hookworms displayed continued egg production for over 2 years post-infection (Fig. S1B). To further confirm infection, PillCam^{TM} capsule endoscopy was performed at week 20 to visualize and enumerate adult worms at the site of infection. Adult parasites were detectable in all participants, with no differences from participants that received cryopreserved larvae (Fig. 2D), and in Fig. 1E representative PillCam^{TM} images are shown.

Eosinophilia was observed as early as 4 weeks post-infection, with peak numbers in the blood occurring by 8 weeks post-infection (Fig. 2F). No correlation was observed between eggs and visualized adult worms (Fig. S1C). No differences were observed in eosinophilia between participants infected with fresh or cryopreserved larvae (Fig. 2F). Given no differences were observed in eggs counts, worm visualization and eosinophil kinetics using cryopreserved larvae, all further analyses were carried out as a combined set.

Hookworm infection increases serum IL-5 and fecal eosinophil-specific degranulation markers

In our study we observed blood eosinophilia in participants infected with *Na,* with peak eosinophilia at week 8 post-infection (Fig. 2F). We analyzed IL-5 levels in serum samples collected over the course of infection and significantly increased serum IL-5 was observed up to 24 weeks post-infection (Fig. 3A), with peak levels observed at 4 weeks post-infection. There was a significant correlation between IL-5 levels and eosinophil count when comparing serum IL-5 at week 4 (preceding the eosinophil peak) and eosinophilia at week 8 (Fig. 3B), however total IL-5 levels did not correlate with total blood eosinophilia (Fig. S2A). No differences were observed in eotaxin (Fig. S2G), a chemokine involved in eosinophil recruitment. We also followed levels eosinophilic cationic protein (ECP) and eosinophil-derived neurotoxin (EDN)*(26)* in fecal samples as a readout of eosinophil activation and degranulation in the intestinal tract. An increase in both ECP and EDN was observed from week 4, with levels peaking at week 8 post-infection (Fig. 3C, 3E). Levels of ECP and EDN positively correlated with blood eosinophil count (Fig. 3D-F), but not with serum IL-5 (Fig. S2B-C). Another inflammatory marker used routinely in a clinical setting is fecal calprotectin (fCal) which is normally exclusively associated with neutrophilic inflammation*(27)*. No differences were observed in blood neutrophils during infection (Fig. 3G) however we did observe a significant transient increase in fCal during the acute phase of infection with levels

remaining within the normal range (Fig. 3G). Interestingly, we did not detect any increase in human neutrophil lipocalin (HNL) (Fig. 3G), a specific neutrophil degranulation marker, indicating that eosinophils might be the major inflammatory cell in the intestine during hookworm infection. Studying cytokine levels in serum, we noticed that individual variation in immune markers is greater than changes induced by the hookworm infection as shown by the PCA (Fig. S2D) and subsequently no significant differences were observed in cytokines involved in type 2 immune responses (Fig. S2E), type 1 immune responses (Fig. S2F), chemokines (Fig. S2G), and serum antibodies (Fig. S2H) when compared to baseline levels. The apparent increase in IL-17A (Fig. S2F) was specific to a participant that developed low eosinophil response upon infection. We also observed an increase in *Na*-specific IgG that reached significance at week 24 post infection (Fig. S2K). No differences were observed when measuring the known immunomodulatory cytokines TGF-β1(Fig. S2I) and IL-10 (Fig. 2SJ). Taken together, these data indicate that infection with 30 iL3 induces a transient increase in IL-5 cytokine levels that is followed by a significant increase in eosinophilia.

Peripheral blood immune cells are unchanged following *N. americanus* infection

We analyzed peripheral blood mononuclear cells (PBMCs) by high dimensional flow cytometry and following an unbiased High Dimensional Analysis approach. Normalization was performed to remove batch to batch variation, we then ran FlowSOM algorithm for clustering the cells and used Uniform Manifold Approximation and Projection (UMAP) to reduce the dimension of the data and to visualize the immune cells in maps. Two panels were used to analyze PBMCs (Fig. S3A-B). According to their receptor expression, we were able to identify $CD4^+$ and $CD8^+$ T cells, γδT cells, T_{REG}, MAIT cells and NKT cells for panel 1 (Fig. 4A), and B cells, dendritic cells, NK cells and monocytes for panel 2 (Fig. 4D). We wanted to investigate if hookworm infection induced perturbation in immune cells apart from

eosinophils. For both panel 1 and panel 2, density plots were generated to visualize any possible change in the main immune cell populations (Fig. 4B and E). We observed a high degree of variability amongst participants, however no significant differences were observed in immune cell frequency (Fig. 4C and F). In general, immune cell variability between individuals was greater than changes induced by the hookworm (Fig. S4A). The two panels allowed us to study several sub-populations in the $CD4^+$ T cell, $CD8^+$ T cell, B cell and DC populations as shown in the gating strategies (Fig. S3A-B), accordingly to markers expression (Fig. S4B and E), and we then overlapped subpopulation using UMAPs in Fig. 4 (Fig. S4C and F). From all sub-populations analyzed no significant differences were observed after hookworm infection as shown by the heat maps (Fig. S4D and H). Taken together these results suggest that infection is well tolerated, and no abnormal immune responses were observed.

Microbiome stability and gut physiology during hookworm infection

We examined fecal samples for microbiome analysis at the indicated time points during infection with *Na*. We visualized beta-diversity by principal component analysis (PCA; Fig 5A) and found inter-individual microbiome composition was the greatest source of variation in the data and no significant changes to beta-diversity induced by hookworm infection (PERMANOVA, $P>0.1$) Microbial community stability (Bray-Curtis dissimilarity relative to D0) (Fig. 5B) and alpha diversity (Shannon diversity index) (Fig. 5C) were not significantly different at any sampled timepoint post infection. Interestingly, participants that experienced moderate GI symptomology (Fig. 5D, showed in red) had a significantly different microbiome from those who experienced mild symptoms or were symptom free (shown in dark blue; PERMANOVA $P < 0.001$) (Fig. 5D), had higher alpha-diversity (Fig. 5E), and a significantly higher relative abundance of the phylum Firmicutes (Fig. 5F, Fig. S5A, Table

S2). At the OTU level we identified 130 taxa that were differentially abundant in participants who experienced moderate GI symptoms (Fig. S5B, Table S3). We observed a linear correlation between fCal levels and alpha diversity (Fig. S5C) and several OTUs with highly significant linear correlations with fCal levels, particularly from the phylum Firmicutes (Fig. S5D). Participants that experienced moderate symptoms did not display higher eosinophil levels at week 4 (Fig. S5E), but they had higher fCal (Fig. S5F), and a trend towards increased ECP and EDN in the feces (Fig. S5G and H respectively). Furthermore, we examined gut motility and physiology using Smartpill^{TM}. We observed a trend towards reduced intestinal transit time at 12 weeks post infection (Fig. S5I) and reduced stomach and small bowel contractility at week 12 (Fig. S5J-K). We found no difference in colon contractility (Fig. S5L). However, we did observe a pH decrease in the small intestine 6-weeks post-infection (Fig. 5G). No significant differences were observed in stomach and colon pH (Fig. S5M-N), and pressure in the stomach and small bowel (Fig. S5O-P).

Changes in the plasma polar metabolome during the acute and chronic phases of hookworm infection

We studied changes in the plasma polar metabolome of participants during the pre-infection (week 0), acute (week 8 – 12) and chronic phases (week 36) using untargeted high-resolution liquid chromatography-mass spectrometry (LC-MS). From the negative and positive electrospray ionization (ESI) modes, 40 and 66 MS (Fig. S6A**)** features were annotated respectively, based on mass spectral database matching with MS-DIAL's built-in metabolomics databases (Data File S4). A total of 12 annotated metabolites including amino acids, amino acid metabolic byproducts and heme metabolism were detected (Fig. 6A). Thus, a total of 94 unique metabolites were annotated, broadly encompassing a diversity of chemical classes including: amino acids, nucleotides, amino acid metabolism products, organic acids,

some dietary-related alkaloids, and exogenous drugs (e.g., paracetamol) (Data File S4). Investigation of the sample variation after correction for run-order using QC samples highlighted excellent quality of the data across both positive and negative ESI modes, as evidenced by tight clustering of pooled participant QC samples in the central area of the plot and well within the variance of the samples (Fig. S6B). Metabolic Set Enrichment Analysis (MSEA) was performed to identify and interpret patterns of metabolite concentration changes during the acute and chronic phases of hookworm infection, relative to the pre-infection phase. Acute phase of infection was significantly associated with the enrichment of metabolites relevant to galactose and tryptophan metabolisms **(**Fig. 6A; Table S4**)**. Other metabolic pathways enriched include metabolism of amino acids (glutamine and glutamate; alanine and aspartate); glyoxylate & dicarboxylate compounds, although these associations were not significant (Table S4). In the chronic phase of infection, we observed a modest enrichment of selenocompound metabolism, biosynthetic pathway of amino acids, metabolism of amino acids, as well as the biosynthesis of ubiquinone and/or terpenoid-quinones (Fig. 6A; Table S5), however enrichment did not reach significance. To interpret the MSEA data in a biological-relevant manner, we performed complementary statistical methods after controlling for potential confounding covariates. We visualized variations amongst all the annotated polar metabolites over the course of infection using PCA (Fig. 6B). Clustering of the datasets were observed at the participant level and variation between participants appears greater than changes induced by hookworm infection. PERMANOVA analysis revealed that the participant gender ("Sex") was the greatest source of variation in the data (PERMANOVA, $p < 0.001$) (Fig. 6B, right panel, Table S6), followed by inter-participants human variation ("Participant ID") (PERMANOVA, $p = 0.072$) (Fig. 6B, Table S6), thus highlighting inherent covariates that need to be considered to correctly identify the main plasma metabolites that changed over hookworm infection. Accordingly, mixed-mode repeated measures two-way ANOVA

analysis, controlling for "sex" and "Participant ID" (Table S7) subsequently revealed that out of the total of 94 annotated polar metabolites, the plasma levels of each of the following metabolites including kynurenine, melibiose, threonic acid, indoxyl sulfate and 5-methoxypsoralen, were significantly different between at least two of the timepoints during the course of hookworm infection. Kynurenine and melibiose are the major contributor to the top two metabolic pathways: galactose and tryptophan metabolisms; respectively (Fig. 6A), during the acute phase of infection. The levels of kynurenine (Fig. 6C, 6D), melibiose (Fig. 6C, Fig. S6C) and indoxyl sulfate (Fig. 6C & Fig. S6D) were increased during the acute phase, before decreasing to levels similar to those of baseline, during the chronic phase of infection. In contrast, levels of the xenobiotic, 5-methoxypsoralen, decreased over the course of hookworm infection (Fig. 6C, Fig. S6E). Threonic acid levels were elevated during the chronic phase of infection, relative to levels observed at baseline (Fig. 6C, Fig. S6F). We observed changes in plasma levels of kynurenine (Fig. 6F), and there was an overall trend of reduction in plasma tryptophan levels during the acute phase, although not reaching statistical significance (Fig. 6G). However, we observed an increase in Kynurenine/Tryptophan ratio, an indicator of increased activity of the rate-limiting enzyme responsible for converting tryptophan to kynurenine; indoleamine 2,3-dioxygenase (IDO), which shunts tryptophan down the kynurenine pathway (Fig. 6H). IDO activity is associated with immunosuppression and regulation. Immune cells can induce IDO activity for example through the expression of cytotoxic T lymphocyte antigen 4 (CTLA-4) that has been shown to be upregulated in helminth-infected population *(11)*. Thus, we analyzed the expression level of CTLA-4 in different T cell subsets of PBMCs: wherein slight increases in CTLA-4 frequency in both $CD25^+$ CD127- $FoxP3^+$ T_{REGS} and $CD4^+$ $CCR4^+$ $CXCR3^-$ T_H2 cells positive for CTLA-4 at week 4 post-infection (Fig. 6I-J) were noticed; with no differences observed in frequencies of CCR6+ CCR4- $CCXR3^-$ T_H9 (Fig. 6K). Interestingly, $T_{REGS,}$ T_H2 and T_H9 had increased

expression (MFI) of CTLA-4 (Fig. 6L-N) in the acute phase of infection, wherein kynurenine/tryptophan ratio was elevated (Fig. 6H). In the T_H2 cell subset (Fig. 6M) the increased expression of CTLA-4 is observed up to week 12 post-infection, with the increase being specific to the $CRTH2^+$ subset (Fig. S6G) as no increase in CTLA-4 MFI was observed in the $CRTH2^-$ subset (Fig. S6G).

DISCUSSION

Since the first trial in 1984*(28)*, experimental hookworm infections have been used in a range of healthy volunteer and human disease settings. To date, host peripheral blood immune responses have been studied due to limitations in obtaining specimens from tissues such as the gastro-intestinal tract. In addition, clinical intervention studies are difficult to develop due to the lack of sufficient knowledge of the immunological interplay between the infecting hookworm, the human host, and the disease context of the host. In this longitudinal study we examined healthy volunteers infected with *Na* for one year. We monitored symptoms and analyzed peripheral immune responses and microbiota. *Na* established a chronic infection in all participants, confirmed by eggs present in feces and adult worm visualization in the intestinal tract. Gastrointestinal symptoms appear to precede egg detection in the feces. Using cryopreservation methods *(25, 29)* we used reanimated cryopreserved larvae in four of our participants, we achieved a successful infection in all four participants and found no significant variation in immune responses. As cryopreservation did not alter infectivity, this method can be used to overcome some of the limitations when performing human controlled infection model such as long-term storage of infective larvae and preparation of defined batches for use in trials. This is the first study demonstrating that cryopreserved hookworm larvae can be used in a clinical study and cryopreservation has the potential to lend itself to cGMP manufacture and biobanking. Our studies show that *Na* infection induces a transient increase in peripheral

blood eosinophils, with eosinophilia peaking at week 8 post-infection. Serum IL-5 levels also increase from week 4 post-infection, preceding the peak in blood eosinophils. Increased levels of the eosinophil degranulation products ECP and EDN were detected in feces and were associated with the increased levels of eosinophils. We used ECP and EDN as a proxy measure for eosinophilic intestinal inflammation, in combination with fCal as measure of neutrophilic inflammation. The timing of the increase in ECP and EDN found in fecal samples suggests that parasites start reaching the gut 4 weeks post infection, causing IL-5 dependent eosinophil responses whose inflammatory mediators are detectable in the feces. fCal increased after infection, but levels remained within the normal limits and did not correlate with neutrophils circulating in the peripheral blood. However, interestingly, calprotectin has been shown to be expressed by eosinophils in mice*(30)* and is elevated in eosinophilic gastrointestinal disorders*(31)* therefore the changes in fCal levels observed in the current study could be of eosinophilic origin. We also measured HNL in feces as a specific marker for neutrophil inflammation*(32)* and detected no increase in this marker, supporting the idea of a local, specific eosinophilic-driven response to hookworm infection. Measuring ECP, EDN, HNL and fCal in feces is a non-invasive method to detect local inflammatory responses during infection. We examined immune cells in the PBMC fraction and other cytokines in serum samples, and only detected serum IL-5 changes following *Na* infection. The transient nature of the increase in gut inflammation could possibly relate to the adult parasite in the gut being mature enough to start modulating the gut immune responses from week 12 of infection. For all parameters analyzed, such as cytokines, immune cells, microbiome, and metabolites, variation between individuals was greater than changes induced by the hookworm, reflecting the challenges involved in studying immune responses in humans*(33)*. We found microbial alpha and beta-diversity to be stable during infection. Only 3 small studies have previously investigated microbial dynamics during a controlled *Na* infection. Our results are consistent with all

previous studies, which have not identified a significant effect of infection on overall community composition or changes to alpha- diversity *(34–36)* . In contrast to us, Ducarmon et al. identified a small increase in microbial richness alone (Chao1) from trial week 8-20, which our study did not replicate. Several studies have identified convincing microbiome signatures associated with natural hookworm infections *(37)*. This seeming discrepancy is likely explained by a multitude of confounding factors such as hookworm burden, hookworm species, lifestyle, and hygiene, among others. Furthermore, the fecal microbiome may not capture the nuanced microbiome dynamics that may occur locally at the site of infection. A convincing understanding of the relationship between the hookworm and the microbiome will likely need larger sample sizes and small intestinal biopsies. Interestingly, we observed that moderate GI symptoms are associated with a more diverse microbiome, higher fCal is associated with increased diversity at the OTU level, and that changes in alpha-diversity are driven by OTUs belonging to the Firmicutes phylum. Similarly, in the longitudinal study by Ducarmon et al. GI symptoms were associated with modest differences in microbial diversity and microbiome stability*(34)*. A deeper understanding of the functional diversity that differentiates between the responders and non-responders will allow us to better understand how the microbiome protects against hookworm-induced GI inflammation. Future studies using shot-gun metagenomics or RNA-sequencing will allow us to better understand microbiome functional potential in this context. We, then, used Smartpill^{TM} and observed a decrease in small bowel pH. The observed pH change could be associated with a change in mucus composition in the small intestine, as reported from mouse studies using *Trichuris muris,* where during the acute and chronic phases of infection different mucin expression is observed as well as glycoprotein hypersecretion driven by IL-13*(38)*. However, pH was measured through Smartpill^{TM} which may not be sensitive enough or located correctly to

measure changes in mucus pH. Nonetheless, the infection is well tolerated due to absence of adverse effects and no significant changes in intestinal physiology.

A novel feature of our study was the analysis of the levels of plasma polar metabolites using high-resolution LC-MS untargeted metabolomics methodology and determining whether they correlate with changes found in PBMC and cytokine immune parameters. MSEA analyses in plasma metabolites highlighted tryptophan metabolism as particularly enriched during the acute phase of infection, with kynurenine being the major contributor. We then considered that the increased plasma kynurenine was complemented partly through the conversion of tryptophan to kynurenine *via* the kynurenine pathway sub-branch of tryptophan metabolism *(39, 40)*. Indeed, we observed changes in plasma kynurenine/tryptophan ratio, indicative of increased activity of the rate-limiting enzyme that converts tryptophan to kynurenine; indoleamine 2,3-dioxygenase (IDO), thought to be part of regulatory mechanisms to protect the host from an over-activated immune system*(41)*. Tryptophan is a substrate for the generation of kynurenine, a metabolite best known for its association with inflammation, immune responses and neurotransmission*(39, 42)*. Activation of the kynurenine pathway is associated with immunosuppression, reducing activity of NK cells, dendritic cells and T cells*(42)*. While we observed an increase in kynurenine in the acute phase of infection, kynurenine biosynthesis is also associated with infection with influenza B and herpex simplex virus*(43)*. Alteration in tryptophan metabolism has been observed in SARS-CoV2 positive subjects*(44)*, thus changes in kynurenine biosynthesis could be a physiological change in response to infection rather than adult parasites inducing immunomodulatory pathway. Our findings pinpoint the need for future studies to conduct more in-depth, targeted metabolomic analyses quantifying changes in various aspects of tryptophan metabolism, particularly downstream metabolites of the kynurenine pathway, to better discern the potential role(s) of tryptophan metabolism products on the immunomodulatory potential of

controlled hookworm infection as well as to distinguish the contrast the changes that are driven by a general response of the host to normal infections. In addition to enrichment of tryptophan metabolism, MSEA analysis also indicated enrichment of galactose metabolism during the acute phase of infection. This enrichment is exclusively driven by increased melibiose levels in plasma. Melibiose, a disaccharide of glucose and galactose, has been linked to suppression of T_H2 cells and induction of oral tolerance in a model of OVA sensitization in mice*(45)* and may thus have involvement in reducing type 2 inflammation (e.g. IL-5 and eosinophils) during hookworm infection. In addition, immune-regulatory pathways have been associated with expansion of T_{REGS} and production of IL-10. In recent years, the surface protein CTLA-4 has been linked to immunomodulation. While we did not observe a general increase in T_{REGS} in peripheral blood, we detected an increase of CTLA-4+ T_{REGS} and T_H2 cells 4 weeks post hookworm infection. Both T_{REGS} and T_H2 cells have higher expression of CTLA-4 as measured by MFI, with T_H2 having increased CTLA-4 expression up to 12-week post infection. Furthermore, we observed an increase in CTLA-4 expression on T_H9 cells, but no increase in CTLA-4^+ T_H9 frequency. Decrease of these populations in the blood could reflect their migration into tissue like lungs and intestine, where *Na* transit through and reside, to reduce inflammatory responses and induce tissue repair. Increase in T_{REGS} has been observed in individuals infected with hookworm, and these cells expressed higher levels of CTLA-4, IL-10, and TGF-β*(46)*. De Ruiter and colleagues did not observe expansion of T_{REGS} in helminth-infected Indonesian, however they showed expansion of CTLA-4+ T_{REGS} and deworming reduced the frequency of this population. Similarly, we observed expansion of CTLA-4+ T_{REGS}, however in our study they decreased over the course of infection, without performing anti-helminth treatment. The main difference could be that multiple infection with different helminths since early age and re-infection over time, as normally happens in helminth endemic areas, drives a constant increase in this T_{REG}

subpopulation. CTLA-4+ T_{REGS} have been shown to be suppressive of antigen-mediated lymphocytes expansion, indicating a potential role in parasite survival and immunomodulation*(46)*, and possibly if we want to develop helminth as a therapeutic agent we should consider multiple re-infection to replenish the modulatory T_{REGS} pool. With this study we wanted to establish a controlled hookworm infection, with confirmation of *Na* infection and safety analysis as primary outcomes, and immune-profiling, microbiome, and metabolites as explorative outcomes. We proved safety and tolerability of infection in a healthy cohort in New Zealand, and the possibility with rigorous sampling to have a global picture of the effect of hookworm infection on the human host. A limitation in this study is that we are focusing on the systemic responses induced by *Na* at specific timepoints, therefore if cytokines are released outside the timepoint selected we will not be able to detect those changes. Similarly, if cytokines/chemokines are released locally in the intestinal tissue, these are unable to be detected. Nonetheless, this controlled infection is a useful tool to further study host-parasite interaction. The single *Na* inoculation used in this study provides a safe and robust method to study systemic and possibly local immune responses against hookworm and the use of helminths is being studied as a possible novel therapeutic agent *(47)*. This controlled human hookworm model provides the base to bring forward hookworm therapies against inflammatory disorders and to build a model to test vaccine efficacy against *Na*.

MATERIALS AND METHODS

Study Design

The primary objective for this study was to establish a cohort of healthy individuals infected with 30 *Na* larvae and profile for 1 year at given time points, gut motility, immune cell, antibody, microbiome and metabolomic responses pre and post infection. This study was

conducted in Wellington, New Zealand. This clinical study was approved by the Health and Disability Ethics Committee (Ethics reference 19/CEN/81) and registered on the Australian New Zealand Clinical Trials Registry (ACTRN12619001129178). Study outline and further information is found in Fig. 1 and Data File S1.

Symptom questionnaire

Participant symptoms were monitored by symptom responses using a modified version of the Talley gut symptom questionnaire*(48)* on weeks 1-12. Symptoms were graded as Mild (Nagging or annoying), Moderate (strong negative influence on daily living) and Severe (disabling) and were self-reported by each participant. In addition, participants were asked to photograph skin reactions during the first 4 weeks of infection.

Parasitology

Two methods were employed for producing *Na* infective larvae. Fresh larvae were produced using fecal-charcoal cultures. Feces collected from a chronically infected volunteer who was screened for communicable agents, were mixed with activated charcoal, and incubated for 7-10 days at 26°C. For "Cryoworms", reanimated cryopreserved larvae were developed to infective larvae using methods previously described*(25, 29)*. Recovered larvae were isolated and washed in 5% iodine solution followed by several washes with sterile distilled water. A dose of 30 *Na* infective larvae (iL3) was used for each participant, administered through two dressings each containing 15 iL3 applied on each forearm. Detection of patency was carried out through presence of *Na* eggs in the feces of infected individuals using the McMaster technique from week 6 following application of larvae.

Whole blood

Whole blood immunophenotyping was performed using 600 µL of heparinized whole blood. RBCs were lysed using in-house made ACK Lysis Solution (ddH_2O with 1mM EDTA,

150mM NH_4Cl, 10mM $NaHCO_3$ at pH 7.4) at 4°C for 10 minutes. Samples were then diluted in PBS to arrest cell lysis, followed by centrifugation at 500g for 5 min at 4°C. The RBC lysis step was repeated once if necessary. Cells were washed twice with PBS and counted. Cells were stained with 1:2000 Zombie NIR Fixable Viability dye (Biolegend) in the dark at room temperature for 15 minutes. Subsequently, cells were stained with the antibody mix (Data file S2) in FACS buffer (PBS + 2% FBS, 0.01% NaN_3) in the presence of 20% Brilliant Stain Buffer Plus (BD Biosciences), at 4°C for 20 minutes. Prior to staining, the antibody mix was filtered through a 0.1µm Centrifugal Filter (Sigma). Subsequently, cells were washed twice with FACS buffer and analyzed on a 5-laser Aurora spectral flow cytometer (Cytek Biosciences). Data was analyzed using FlowJo v10.7.1 and Prism V8 (GraphPad Software Inc.).

PBMC isolations and analysis

Peripheral blood mononuclear cells (PBMCs) were isolated from heparinized whole blood by SepMate™ PBMC Isolation Tube (STEMCELL Technologies). Briefly, whole blood was diluted 1:1 in PBS +2% FBS, added to the SepMate™ PBMC Isolation Tube containing 15ml of Lymphoprep (STEMCELL Technologies) and centrifuged at 1200g for 12 minutes at RT. Collected PBMC were washed three times with PBS + 2% FBS and cryopreserved in FBS + 10% DMSO. Cryovials containing PBMC suspension were transferred to a Corning® CoolCell® Container, which was placed at -80°C overnight. Cryovials were then stored in liquid nitrogen until analysis. On day of analysis, thawed cells were resuspended in PBS + 2% FBS, counted and for optimal protocol up to $5x10^6$ cells were resuspended in FACS buffer and used for staining. Two antibody panels were designed to assess 1) T cell subsets, NK T cells, MAIT cells and 2) B cells, NK cells, Monocytes and Dendritic cells. Details on antibodies used and gating strategies are listed in Data File S2 and Figure S3. PBMCs were incubated with 1:2000 Zombie NIR Fixable Viability dye (Biolegend) at room temperature

for 20 minutes. After washing, cells were incubated with 1:40 FC block (Biolegend) for 10 minutes at room temperature.

For panel 1, cells were surface stained for CD1d and MR1 tetramers for 15 minutes at 37°C, washed and sequentially stained for CD25, TCRγδ, CXCR3, CCR10, CCR6, CCR4, CCR7 for 5 minutes each at 37°C. For panel 2, cells were sequentially stained for CXCR5 and CCR7 for 5 minutes each at 37°C. After sequential staining cells were incubated with surface receptor mix for 20 minutes at room temperature in the presence of Brilliant Buffer Plus (BD Biosciences) and Monocyte Block (1:30, Biolegend) only for panel 2. Cells were fixed and permeabilized with FoxP3/Transcription Factor Staining Buffer Set (eBioscience) for 30 minutes at room temperature and subsequently incubated with FC block (1:40, Biolegend) for 10 minutes at room temperature. Cells were washed in Permeabilization Buffer (eBioscience), incubated with intracellular antibody mix for 40 minutes on a shaking plate at room temperature. Cells were then resuspended in FACS buffer and analyzed on a 5-laser Aurora spectral flow cytometer (Cytek Biosciences).

PillCam

Hookworm visualization in the small bowel was carried out using the PillCam™ SB3 Capsule Endoscopy System (Medtronic). Capsules were administered by supervision of trained staff from The Rutherford Clinic (Lower Hutt, New Zealand). Participants were instructed to drink a bowel prep (Klean-Prep), maintain a clear liquid diet from midday prior to administration and fast from midnight prior to administration. PillCam™ video recordings were analyzed using RAPID Reader software by two people separately, then final numbers of worms visualized were discussed and finalized. Data were tabulated and graphically presented using Prism V8 (GraphPad Software Inc.).

Smartpill delivery

Motility, temperature, pH and pressure of gastrointestinal tracts were measured at indicated timepoints using the SmartPill™ Motility Monitoring Capsule and SmartPill™ Software v3.1 (Given Imaging and Medtronic). Capsules were administered by trained staff according to the User Manual (DOC-4092-01 November 2017) and software instructions. Participants were instructed to fast from food and drink for 8 hours before a test, ate a SmartBar™ prior to capsule ingestion and were instructed to refrain from eating until 6 hours into the test. Tests were analyzed using the software's Test Analysis Wizard.

Microbiome

Fecal samples were self-collected using a disposable toilet accessory (DNA Genotek, Canada) and samples were placed into OMNIgene.GUT tubes (DNA Genotek, Canada) according to manufacturer's instructions. Samples were placed in chiller-bags containing an ice-pack and delivered to the laboratory within 24 hours of collection. OMNIgene.GUT tubes were stored at –80°C until processing. DNA was extracted from fecal samples using the Qiagen MagAttract PowerSoil DNA KF Kit optimized for the Thermofisher KingFisher robot. DNA quantification and quality checks were done via Qubit. 16s rDNA marker gene (V4) was amplified using the high-fidelity Phusion polymerase using dual-barcoded primers*(49)* and PCR products were verified by gel electrophoresis. PCR reactions were cleaned and normalized using the SequalPrep 96-well Plate Kit. Library samples were pooled and sequenced on the Illumina Miseq. Fastq files were quality filtered and clustered into 97% similarity operational taxonomic units (OTUs) using the mothur software package*(49)*. Representative OTU sequences were assigned taxonomic classification using a Bayesian classifier against the Ribosomal database project (RDP) database*(50)*. Before filtering, alpha diversity (Shannon measure) was calculated and plotted using Phyloseq*(51)*. Data was centered log-ratio (CLR) transformed and filtered. Data was further analyzed in R using

custom scripts and plotted using ggplot2*(52)*.

Plasma Metabolomics analysis

Plasma samples for metabolomics analysis were sent to AgResearch (Palmerston North, NZ). For acute phase of infection, week 8 samples were analyzed except for 2 participants for which week 12 samples were analyzed due to inability of collecting week 8 samples due to COVID-19 restrictions in New Zealand. For chronic phase week 36 samples were analyzed. Polar metabolites were extracted from participant plasma samples as previously described *(53)*. Briefly, processed plasma was placed into an HPLC vial for LC-MS using HILIC chromatography. Pooled quality control (QC) samples were prepared by pooling together 50 µL of each participant plasma sample. QC were analyzed alongside samples to allow for signal normalization to correct for any loss of signal across the analytical batch.

Polar metabolites extracted from plasma samples were analyzed using a Shimadzu LCMS-9030 mass spectrometer equipped with a Shimadzu Nexera-x2 UHPLC system. Data were captured, converted and peaks were then annotated using the DIA MS/MS data collected against the built-in human metabolite library containing 13,303 MS/MS spectra*(54)*. The resultant peak intensity table underwent run-order correction and normalization using pooled QC samples and the locally weighted scatterplot smoother (LOWESS) regression model. Plasma metabolome data (Data File S4**)** underwent log-transformation and autoscaling prior to the following analyses: (i) Metabolite Set Enrichment Analysis (MSEA) using the Quantitative Enrichment Analysis (QEA) module on MetaboAnalyst 5.0 *(55)*; (ii) principal component analysis (PCA); (iii) permutational multivariate analysis of variance (PERMANOVA); (iv) mixed-mode repeated measures two-way ANOVA with Dunnett's post-hoc multiple comparison tests, all analyzed using R software and/or GraphPad Prism (Version 8).

ELISA for fecal degranulation products

For extraction of ECP, EDN and HNL from feces the granule protein extraction protocol was used as described elsewhere *(56)*. Feces samples were self-collected and immediately frozen at -80°C. On the day of processing feces samples were thawed overnight in the refrigerator or at room temperature for 1 hour. Feces was weighted and diluted five times in extraction buffer consisting of phosphate-buffered saline, pH 7.4, supplemented with 10-mmol/L ethylenediamin- etretraacetic acid, 0.2% *N*-cetyl-*N,N,N*-trimethylammonium bromide (CTAB)(Sigma), 20% glycerol (Sigma), 0.05% Tween20, and 1% bovine serum albumin. The mixture was homogenized using a homogenizer mixer until a homogenous solution was obtained. After incubation at 4°C for 30-45 min and mixing, the homogenate was centrifuged at 4,000g for 30 min at 5°C. The supernatant was aliquoted and frozen at -20°C for later ELISA analysis. For each sample a separate tube of the diluted homogenate was weighed and centrifuged. By weighing the pellet obtained after discarding the supernatant, a measure of semidry weight was obtained. Fecal ECP, EDN and HNL were measured by ELISA (Diagnostics Development AB, Uppsala, Sweden) according to the manufacturer's protocol. The levels of markers in feces were adjusted for water content and expressed as micrograms per gram of semidry faeces. For extraction of fecal calprotectin CALEX Cap devices (Bühlmann Laboratories, USA) were used according to the manufacturer's protocol. Fecal calprotectin was measured by fCal ELISA (Bühlmann Laboratories, USA) according to the manufacturer's protocol.

ELISA/Multiplex Assays (Serologic analysis)

Plasma was separated from heparinized whole blood by centrifugation at 2000g for 15 minutes at 4ºC. Serum was separated from clotted blood by centrifugation at 2000g for 10 minutes at 4ºC. Plasma and serum were stored at -80°C until analysis.

For serological analysis, samples were analyzed using MILLIPLEX® MAP Kits purchased from Merck-Millipore. Serum samples were tested for IgE, IgG isotypes, IgA, IgM,

RANTES, BCA-1, Eotaxin-3, TSLP, IL-33, Eotaxin, IFNγ, IL-1β, IL-3, IL-4, IL-5, IL-6, IL-8, IL-10, IL-12.p70, IL-13, IL-17A, TNFα, and TGF-β, according to manufacturer instruction. Briefly, 25ul of diluent containing antibody-coupled beads was added to a black clear-bottomed 96-well plate (Merck-Millipore). Diluted serum was added to the plate and incubated for 1 or 2 hours according to the kit protocol. Plates were washed, incubated with detection antibody, followed by another wash and incubation with Streptavidin-Phycoerythrin (Merck-Millipore). The plate was placed on a magnetic plate holder (Bio-Rad) for 1 minute before 35 µL of fluid was removed from wells and 150 µL sheath fluid (Thermo Fisher Scientific) added. Finally, the plate was analyzed in a Luminex 200 array reader (Merck-Millipore), and results were determined against commercial standards (Merck-Millipore) using the Luminex xPONENT® software. Cytokines under the limit of detection not shown in the result section.

For *Na*-specific IgG ELISA, samples were analyzed following the protocol previously described*(20)*. Briefly, somatic extract was prepared using approximately 75000 iL_3 in 500 µl lysis buffer (3 M urea, 0.2% SDS, 1% Triton X-100, 50 mM Tris-HCl). Larvae were homogenized by hand using a tissue grinder and subsequently sonicated at 4 °C. Sonicated larvae were centrifuged at 10000 g at 4 °C for 10 minutes, supernatants collected, and protein quantified by BCA assay (Pierce). 96-well Nunc MaxiSorp ELISA plates (Thermo Fisher Scientific) were coated with 5 µg/mL somatic extract overnight at 4°C. Plates were washed with PBST/0.05% BSA and blocked with PBST/5% BSA for 2 hours at room temperature with shaking (400 revolutions per minute/rpm). Plates were washed as above and incubated with 50 µL participant sera diluted at 1:100 in PBST/1% BSA for 1 hour at room temperature with shaking (400 rpm). Plates were washed as above and incubated with 50 µL goat anti-human IgG-horseradish peroxidase (Sigma-Aldrich) diluted at 1:5000 in PBST/1% BSA for 1 hour at room temperature with shaking. Plates were then washed and incubated with TMB

substrate (Thermo Fisher Scientific) for 5 minutes. The reaction was stopped with an equal volume of 1M H_2SO_4 and absorbance was measured at 450 nm through Infinite® M1000 plate reader using i-control™ 2.0 software (Tecan).

Analysis, visualization, and Statistical analysis

Whole blood flow cytometry data was analyzed using FlowJo software. PBMCs flow cytometry data was batch-to-batch normalized using CytoNorm algorithm in R studio. Data was analyzed using flowSOM clustering algorithm and UMAP algorithm as a visualization tool using the cloud-based OMIQ software (San Francisco, USA). Heatmaps and PCA plots were generated using R software or OMIQ and modified in Adobe Illustrator. Statistical tests were performed in R or using Graphpad Prism version 9 as indicated in each figure legends. D'Agostino & Pearson normality test were performed for each dataset before running One-way ANOVA.

Supplementary Materials

Figure S1: Skin reaction, egg production and worm count

Figure S2: Eosinophils correlation, cytokines, and immunoglobulins profiling

Figure S3: PBMCs gating strategies

Figure S4: Immuno-profiling of PBMC subpopulations

Figure S5: Microbial diversity and gut physiology

Figure S6: Changes in plasma levels of four polar metabolites and changes in CTLA-4 MFI of CRTH2+ or CRTH2- CTLA-4+ Th2 cells over the course of hookworm infection

Data file S1: Participant Inclusion/exclusion criteria

Data file S2: List of flow cytometry antibodies

Data file S3: OTUs data file.

Data file S4: Accurate masses and retention times of all annotated metabolites detected in plasma as analyzed using negative and positive electrospray ionization modes.

Data file S5: Primary data.

Table S1: Demographic Information

Table S2: Microbiome Dataset

Table S3: Microbiome Dataset Phylum and Symptoms score

Table S4. Metabolic Set Enrichment Analysis (MSEA) statistics comparing metabolic pathways enriched during the "acute phase" of hookworm infection, relative to baseline (i.e., "pre-infection phase")

Table S5: Metabolic Set Enrichment Analysis (MSEA) statistics comparing metabolic pathways enriched during the "chronic phase" of hookworm infection, relative to baseline (i.e. "pre-infection phase")

Table S6: PERMANOVA Analysis identifying "Sex" and "Participant ID" as important covariates to control for in downstream statistical analyses

Table S7: Two-way, repeated-measures Mixed ANOVA analysis statistics, controlling for "sex" and "participant ID" as covariates.

Movie S1: PillCam^{TM} video from hookworm-infected volunteer

References and Notes

1. D. I. Pritchard, R. J. Quinnell, M. Moustafa, P. G. McKean, A. F. G. Siater, A. Raiko, A. E. Keymer, Hookworm (necator americanus) infection and storage iron depletion. *Trans. R. Soc. Trop. Med. Hyg.* (1991), doi:10.1016/0035-9203(91)90038-Z.

2. S. M. Bartsch, P. J. Hotez, L. Asti, K. M. Zapf, M. E. Bottazzi, D. J. Diemert, B. Y. Lee, The Global Economic and Health Burden of Human Hookworm Infection. *PLoS Negl. Trop. Dis.* (2016), doi:10.1371/journal.pntd.0004922.

3. A. Zawawi, K. J. Else, Soil-Transmitted Helminth Vaccines: Are We Getting Closer? *Front. Immunol.* **11**, 576748 (2020).

4. M. Zarowiecki, M. Berriman, What helminth genomes have taught us about parasite evolution*Parasitology* (2015), doi:10.1017/S0031182014001449.

5. D. I. Pritchard, D. Diemert, M. E. Bottazzi, J. M. Hawdon, R. Correa-Oliveira, J. M. Bethony, Controlled Infection of Humans with the Hookworm Parasite Necator americanus to Accelerate Vaccine Development : The Human Hookworm Vaccination/Challenge Model (HVCM). *Curr. Top. Microbiol. Immunol.* (2021), doi:10.1007/82_2021_237.

6. M. Yazdanbakhsh, P. G. Kremsner, R. Van Ree, Parasites and the hygiene hypothesis. *Science (80-.).* (2002).

7. P. R. Chapman, P. Giacomin, A. Loukas, J. S. McCarthy, Experimental human hookworm infection: a narrative historical review. *PLoS Negl. Trop. Dis.* **15**, e0009908 (2021).

8. P. J. Cooper, M. E. Chico, L. C. Rodrigues, M. Ordonez, D. Strachan, G. E. Griffin, T. B. Nutman, Reduced risk of atopy among school-age children infected with geohelminth parasites in a rural area of the tropics. *J. Allergy Clin. Immunol.* **111**, 995–1000 (2003).

9. A. H. van den Biggelaar, R. van Ree, L. C. Rodrigues, B. Lell, A. M. Deelder, P. G. Kremsner, M. Yazdanbakhsh, Decreased atopy in children infected with Schistosoma haematobium: a role for parasite-induced interleukin-10. *Lancet (London, England)* **356**, 1723–1727 (2000).

10. A. H. J. van den Biggelaar, L. C. Rodrigues, R. van Ree, J. S. van der Zee, Y. C. M. Hoeksma-Kruize, J. H. M. Souverijn, M. A. Missinou, S. Borrmann, P. G. Kremsner, M. Yazdanbakhsh, Long-term treatment of intestinal helminths increases mite skin-test reactivity in Gabonese schoolchildren. *J. Infect. Dis.* **189**, 892–900 (2004).

11. K. de Ruiter, S. P. Jochems, D. L. Tahapary, K. A. Stam, M. König, V. van Unen, S. Laban, T. Höllt, M. Mbow, B. P. F. Lelieveldt, F. Koning, E. Sartono, J. W. A. Smit, T. Supali, M. Yazdanbakhsh, Helminth infections drive heterogeneity in human type 2 and regulatory cells. *Sci. Transl. Med.* (2020), doi:10.1126/scitranslmed.aaw3703.

12. D. Blount, D. Hooi, J. Feary, A. Venn, G. Telford, A. Brown, J. Britton, D. Pritchard, Immunologic profiles of persons recruited for a randomized, placebo-controlled clinical trial of hookworm infection. *Am. J. Trop. Med. Hyg.* (2009), doi:10.4269/ajtmh.2009.09-0237.

13. D. Elias, S. Britton, A. Aseffa, H. Engers, H. Akuffo, Poor immunogenicity of BCG in helminth infected population is associated with increased in vitro TGF-β production. *Vaccine* **26**, 3897–3902 (2008).

14. F. Vacca, G. Le Gros, Tissue-specific immunity in helminth infections. *Mucosal Immunol.* , 1–12 (2022).

15. L. J. Wammes, F. Hamid, A. E. Wiria, B. de Gier, E. Sartono, R. M. Maizels, A. J. F. Luty, Y. Fillié, G. T. Brice, T. Supali, H. H. Smits, M. Yazdanbakhsh, Regulatory T cells in

human geohelminth infection suppress immune responses to BCG and Plasmodium falciparum. *Eur. J. Immunol.* **40**, 437–442 (2010).

16. K. Mortimer, A. Brown, J. Feary, C. Jagger, S. Lewis, M. Antoniak, D. Pritchard, J. Britton, Dose-ranging study for trials of therapeutic infection with necator Americanus in humans. *Am. J. Trop. Med. Hyg.* (2006), doi:10.4269/ajtmh.2006.75.914.

17. J. Feary, A. Venn, A. Brown, D. Hooi, F. H. Falcone, K. Mortimer, D. I. Pritchard, J. Britton, Safety of hookworm infection in individuals with measurable airway responsiveness: A randomized placebo-controlled feasibility study. *Clin. Exp. Allergy* (2009), doi:10.1111/j.1365-2222.2009.03187.x.

18. J. R. Feary, A. J. Venn, K. Mortimer, A. P. Brown, D. Hooi, F. H. Falcone, D. I. Pritchard, J. R. Britton, Experimental hookworm infection: A randomized placebo-controlled trial in asthma. *Clin. Exp. Allergy* (2010), doi:10.1111/j.1365-2222.2009.03433.x.

19. S. Gaze, H. J. McSorley, J. Daveson, D. Jones, J. M. Bethony, L. M. Oliveira, R. Speare, J. S. McCarthy, C. R. Engwerda, J. Croese, A. Loukas, Characterising the mucosal and systemic immune responses to experimental human hookworm infection. *PLoS Pathog.* (2012), doi:10.1371/journal.ppat.1002520.

20. P. R. Chapman, R. Webster, P. Giacomin, S. Llewellyn, L. Becker, M. S. Pearson, F. De Labastida Rivera, P. O'Rourke, C. R. Engwerda, A. Loukas, J. S. McCarthy, Vaccination of human participants with attenuated Necator americanus hookworm larvae and human challenge in Australia: a dose-finding study and randomised, placebo-controlled, phase 1 trial. *Lancet. Infect. Dis.* **21**, 1725–1736 (2021).

21. J. Croese, J. O'Neil, J. Masson, S. Cooke, W. Melrose, D. Pritchard, R. Speare, A proof of concept study establishing Necator americanus in Crohn's patients and reservoir donors [8]*Gut* (2006), doi:10.1136/gut.2005.079129.

22. J. Croese, G. C. Miller, L. Marquart, S. Llewellyn, R. Gupta, L. Becker, A. D. Clouston, C. Welch, J. Sidorenko, L. Wallace, P. M. Visscher, M. L. Remedios, J. S. McCarthy, P. O'Rourke, G. Radford-Smith, A. Loukas, M. Norrie, J. W. Masson, R. B. Gearry, T. Rahman, P. R. Giacomin, Randomized, Placebo Controlled Trial of Experimental Hookworm Infection for Improving Gluten Tolerance in Celiac Disease. *Clin. Transl. Gastroenterol.* (2020), doi:10.14309/ctg.0000000000000274.

23. H. J. McSorley, S. Gaze, J. Daveson, D. Jones, R. P. Anderson, A. Clouston, N. E. Ruyssers, R. Speare, J. S. McCarthy, C. R. Engwerda, J. Croese, A. Loukas, Suppression of inflammatory immune responses in celiac disease by experimental hookworm infection. *PLoS One* (2011), doi:10.1371/journal.pone.0024092.

24. R. Tanasescu, C. R. Tench, C. S. Constantinescu, G. Telford, S. Singh, N. Frakich, D. Onion, D. P. Auer, B. Gran, N. Evangelou, Y. Falah, C. Ranshaw, C. Cantacessi, T. P. Jenkins, D. I. Pritchard, Hookworm Treatment for Relapsing Multiple Sclerosis. *JAMA Neurol.* (2020), doi:10.1001/jamaneurol.2020.1118.

25. T. J. Nolan, V. M. Bhopale, Z. Megyeri, G. A. Schad, Cryopreservation of human hookworms. *J. Parasitol.* (1994), doi:10.2307/3283205.

26. S. P. Hogan, H. F. Rosenberg, R. Moqbel, S. Phipps, P. S. Foster, P. Lacy, A. B. Kay, M. E. Rothenberg, Eosinophils: biological properties and role in health and disease.*Clin. Exp. allergy J. Br. Soc. Allergy Clin. Immunol.* **38**, 709–750 (2008).

27. F. S. Lehmann, E. Burri, C. Beglinger, The role and utility of faecal markers in inflammatory bowel disease. *Therap. Adv. Gastroenterol.* **8**, 23–36 (2015).

28. B. L. Cline, M. D. Little, R. K. Bartholomew, N. A. Halsey, Larvicidal activity of albendazole against Necator americanus in human volunteers. *Am. J. Trop. Med. Hyg.* **33**, 387–394 (1984).

29. K. F. O'Connell, An Improved Method for Freezing Nematodes Using a Trehalose-DMSO Cryoprotectant (2017) (available at http://wbg.wormbook.org/2017/07/11/an-improved-method-for-freezing-nematodes-using-a-trehalose-dmso-cryoprotectant/).

30. H. Reichman, I. Moshkovits, M. Itan, M. Pasmanik-Chor, T. Vogl, J. Roth, A. Munitz, Transcriptome profiling of mouse colonic eosinophils reveals a key role for eosinophils in the induction of s100a8 and s100a9 in mucosal healing. *Sci. Rep.* **7**, 7117 (2017).

31. I. H. Yoo, J. M. Cho, J. Y. Joo, H. R. Yang, Fecal Calprotectin as a Useful Non-Invasive Screening Marker for Eosinophilic Gastrointestinal Disorder in Korean Children. *J. Korean Med. Sci.* **35**, e120 (2020).

32. P. Venge, L. Douhan-Håkansson, D. Garwicz, C. Peterson, S. Xu, K. Pauksen, Human Neutrophil Lipocalin as a Superior Diagnostic Means To Distinguish between Acute Bacterial and Viral Infections. *Clin. Vaccine Immunol.* **22**, 1025–1032 (2015).

33. A. Liston, S. Humblet-Baron, D. Duffy, A. Goris, Human immune diversity: from evolution to modernity. *Nat. Immunol.* (2021), doi:10.1038/s41590-021-01058-1.

34. Q. R. Ducarmon, M. A. Hoogerwerf, J. J. Janse, A. R. Geelen, J. P. R. Koopman, R. D. Zwittink, J. J. Goeman, E. J. Kuijper, M. Roestenberg, Dynamics of the bacterial gut microbiota during controlled human infection with Necator americanus larvae. *Gut Microbes* **12**, 1–15 (2020).

35. T. P. Jenkins, D. I. Pritchard, R. Tanasescu, G. Telford, M. Papaiakovou, R. Scotti, A. Cortés, C. S. Constantinescu, C. Cantacessi, Experimental infection with the hookworm, Necator americanus, is associated with stable gut microbial diversity in human volunteers with relapsing multiple sclerosis. *BMC Biol.* **19**, 1–17 (2021).

36. C. Cantacessi, P. Giacomin, J. Croese, M. Zakrzewski, J. Sotillo, L. McCann, M. J. Nolan, M. Mitreva, L. Krause, A. Loukas, Impact of experimental hookworm infection on the human gut microbiota. *J. Infect. Dis.* **210**, 1431–1434 (2014).

37. P. Loke, S. C. Lee, O. O. Oyesola, Effects of helminths on the human immune response and the microbiome. *Mucosal Immunol.* (2022), doi:10.1038/s41385-022-00532-9.

38. S. Z. Hasnain, D. J. Thornton, R. K. Grencis, Changes in the mucosal barrier during acute and chronic Trichuris muris infection. *Parasite Immunol.* **33**, 45–55 (2011).

39. J. Savitz, The kynurenine pathway: a finger in every pie. *Mol. Psychiatry* **25**, 131–147 (2020).

40. A. Agus, J. Planchais, H. Sokol, Gut Microbiota Regulation of Tryptophan Metabolism in Health and Disease. *Cell Host Microbe* **23**, 716–724 (2018).

41. D. H. Munn, A. L. Mellor, Indoleamine 2,3 dioxygenase and metabolic control of immune responses. *Trends Immunol.* **34**, 137–143 (2013).

42. I. Cervenka, L. Z. Agudelo, J. L. Ruas, Kynurenines: Tryptophan's metabolites in exercise, inflammation, and mental health. *Science* **357** (2017), doi:10.1126/science.aaf9794.

43. L. Gaelings, S. Söderholm, A. Bugai, Y. Fu, J. Nandania, B. Schepens, M. B. Lorey, J. Tynell, L. Vande Ginste, R. Le Goffic, M. S. Miller, M. Kuisma, V. Marjomäki, J. De Brabander, S. Matikainen, T. A. Nyman, D. H. Bamford, X. Saelens, I. Julkunen, H. Paavilainen, V. Hukkanen, V. Velagapudi, D. E. Kainov, Regulation of kynurenine

biosynthesis during influenza virus infection.*FEBS J.* **284**, 222–236 (2017).

44. T. Thomas, D. Stefanoni, J. A. Reisz, T. Nemkov, L. Bertolone, R. O. Francis, K. E. Hudson, J. C. Zimring, K. C. Hansen, E. A. Hod, S. L. Spitalnik, A. D'Alessandro, COVID-19 infection alters kynurenine and fatty acid metabolism, correlating with IL-6 levels and renal status. *JCI insight* **5** (2020), doi:10.1172/jci.insight.140327.

45. K. Tomita, T. Nagura, Y. Okuhara, H. Nakajima-Adachi, N. Shigematsu, T. Aritsuka, S. Kaminogawa, S. Hachimura, Dietary melibiose regulates th cell response and enhances the induction of oral tolerance. *Biosci. Biotechnol. Biochem.* **71**, 2774–2780 (2007).

46. N. D. Ricci, J. A. Fiúza, L. L. Bueno, G. G. L. Cançado, P. H. Gazzinelli-Guimarães, V. G. Martins, L. F. Matoso, R. R. C. de Miranda, S. M. Geiger, R. Correa-Oliveira, A. Gazzinelli, D. C. Bartholomeu, R. T. Fujiwara, Induction of CD4(+)CD25(+)FOXP3(+) regulatory T cells during human hookworm infection modulates antigen-mediated lymphocyte proliferation. *PLoS Negl. Trop. Dis.* **5**, e1383 (2011).

47. P. R. Chapmanid, P. Giacominid, A. Loukas, J. S. Mccarthyid, J. Cotton, Ed. Experimental human hookworm infection: a narrative historical review. *PLoS Negl. Trop. Dis.* **15**, e0009908 (2021).

48. E. Rey, G. R. 3rd Locke, H.-K. Jung, A. Malhotra, R. S. Choung, T. J. Beebe, C. D. Schleck, A. R. Zinsmeister, N. J. Talley, Measurement of abdominal symptoms by validated questionnaire: a 3-month recall timeframe as recommended by Rome III is not superior to a 1-year recall timeframe. *Aliment. Pharmacol. Ther.* **31**, 1237–1247 (2010).

49. J. J. Kozich, S. L. Westcott, N. T. Baxter, S. K. Highlander, P. D. Schloss, Development of a dual-index sequencing strategy and curation pipeline for analyzing amplicon sequence data on the MiSeq Illumina sequencing platform. *Appl. Environ. Microbiol.* **79**, 5112–5120 (2013).

50. J. R. Cole, Q. Wang, J. A. Fish, B. Chai, D. M. McGarrell, Y. Sun, C. T. Brown, A. Porras-Alfaro, C. R. Kuske, J. M. Tiedje, Ribosomal Database Project: data and tools for high throughput rRNA analysis. *Nucleic Acids Res.* **42**, D633-42 (2014).

51. P. J. McMurdie, S. Holmes, phyloseq: an R package for reproducible interactive analysis and graphics of microbiome census data. *PLoS One* **8**, e61217 (2013).

52. H. Wickham, *ggplot2* (Springer New York, 2009).

53. K. Fraser, N. C. Roy, L. Goumidi, A. Verdu, P. Suchon, F. Leal-Valentim, D.-A. Trégouët, P.-E. Morange, J.-C. Martin, Plasma Biomarkers and Identification of Resilient Metabolic Disruptions in Patients With Venous Thromboembolism Using a Metabolic Systems Approach. *Arterioscler. Thromb. Vasc. Biol.* **40**, 2527–2538 (2020).

54. H. Tsugawa, T. Cajka, T. Kind, Y. Ma, B. Higgins, K. Ikeda, M. Kanazawa, J. VanderGheynst, O. Fiehn, M. Arita, MS-DIAL: data-independent MS/MS deconvolution for comprehensive metabolome analysis. *Nat. Methods* **12**, 523–526 (2015).

55. Z. Pang, G. Zhou, J. Ewald, L. Chang, O. Hacariz, N. Basu, J. Xia, Using MetaboAnalyst 5.0 for LC-HRMS spectra processing, multi-omics integration and covariate adjustment of global metabolomics data. *Nat. Protoc.* **17**, 1735–1761 (2022).

56. C. G. B. Peterson, E. Eklund, Y. Taha, Y. Raab, M. Carlson, A new method for the quantification of neutrophil and eosinophil cationic proteins in feces: establishment of normal levels and clinical application in patients with inflammatory bowel disease. *Am. J. Gastroenterol.* **97**, 1755–1762 (2002).

57. Y. Benjamini, Y. Hochberg, Controlling the False Discovery Rate: A Practical and Powerful Approach to Multiple Testing. *J. R. Stat. Soc. Ser. B* **57**, 289–300 (1995).

Acknowledgments:

We would like to acknowledge the Hugh Green Cytometry Centre for their help with the cytometry data and Dr. Karl Fraser (AgResearch Ltd, Palmerston North, New Zealand) for providing help and insightful discussion in plasma metabolomics analyses. We would also like to acknowledge Prof. Alex Loukas and Dr. Paul Giacomin for insightful discussion.

Funding:

Health Research Council Independent Research Organization grant (ref 18/1003) and the Woodrose family.

Author contributions:
Conceptualization: MC, GLG, SI
Funding Acquisition: GLG
Formal Analysis: FV, BL, SLN, AC, LFF, JST, TCM, MC
Investigation: FV, BL, SLN, KM, BY, TTK, JM
Writing – Original Draft: FV
Writing – review & editing: FV, BL, SLN, TCM, LFF, AC, JST, OG, GLG, MC, SI
Project administration: MC

Competing interests:

Authors declare that they have no competing interest.

Data and materials availability:

All data are available in the main text or the supplementary materials.

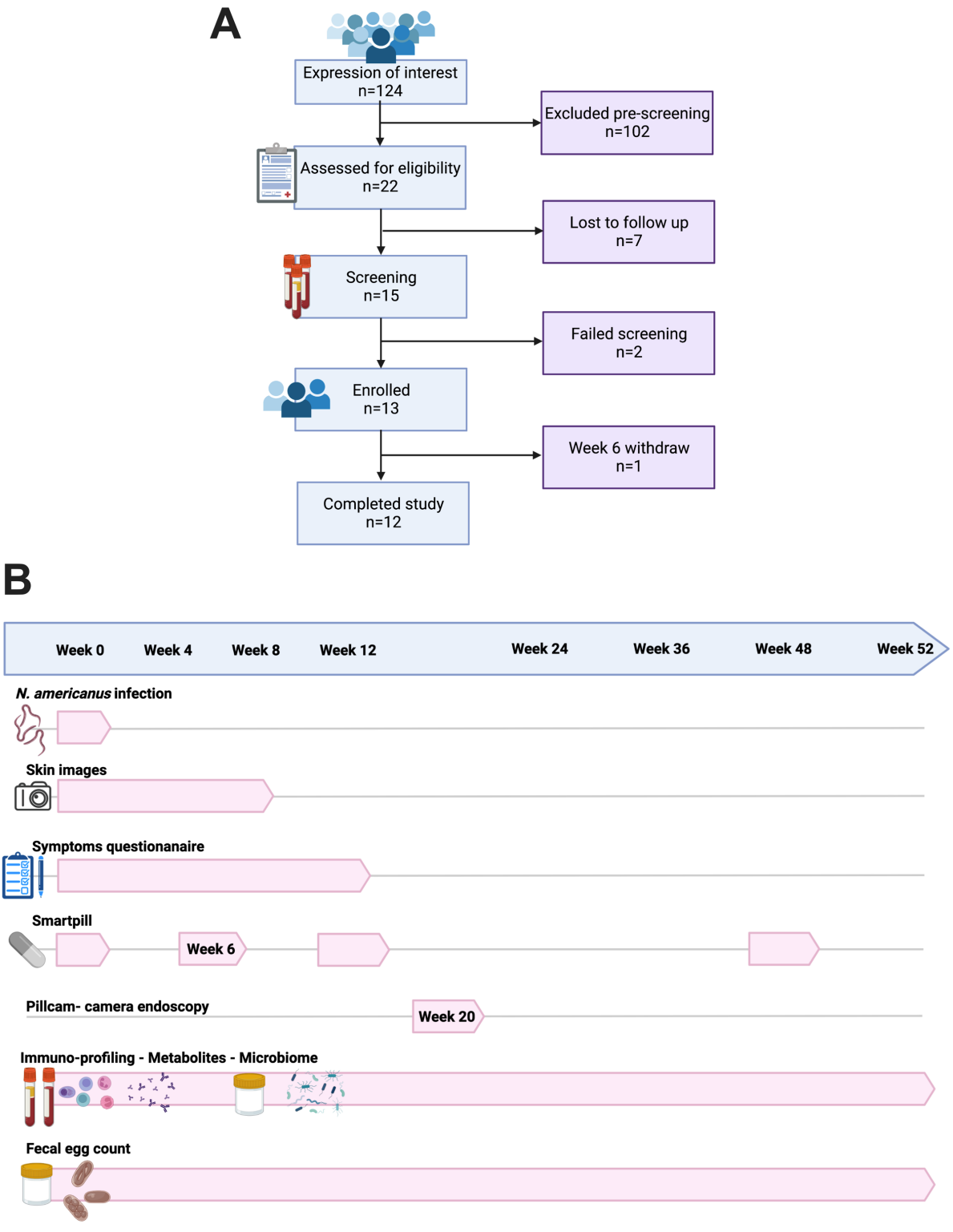

Figure 1: Trial profile and study design

(A) Schematic representation of the recruitment and eligibility process. Eligibility criteria described in Data File S1. (B) Study design with sample collection. Created with BioRender.com

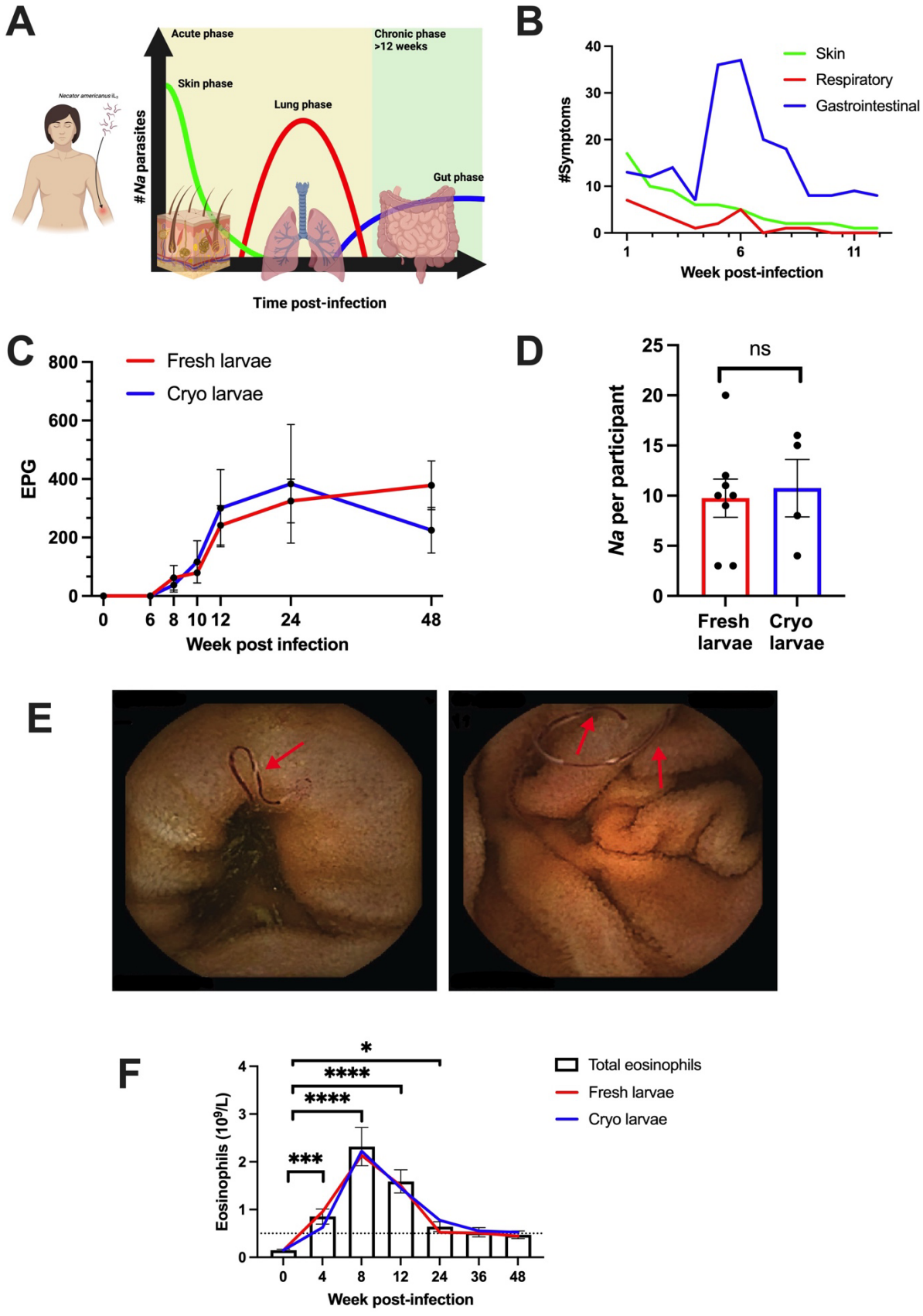

Figure 2: *Necator americanus* infection induces site-specific symptoms and eosinophilia

(A) Schematic representation of phases during hookworm infection investigated in this study. Created with BioRender.com (B) Self-reported symptoms divided by organs affected by parasite traverse in the host. (C) Plot showing mean ± SEM eggs count measured from fresh stool samples divided by participants that received fresh (red line) or cryopreserved (blue line) larvae. (D) Graph showing adult hookworm counted in the gastrointestinal tract with Pillcam^{TM} endoscopy divided by participants that received fresh (red) and cryopreserved larvae (blue). Showed is average from two independent counting. (E) Representative images of Pillcam^{TM} endoscopy showing hookworm (red arrow) in the intestinal tract. (F) Bar graph showing mean ± SEM of peripheral blood eosinophil count. Lines showing eosinophils count in participants infected with fresh (red line) or cryopreserved (blue line) larvae. Results were analysed with One-way ANOVA using Friedman test with Dunn's multiple comparison test. p=*<0.05, **<0.005,****<0.0001

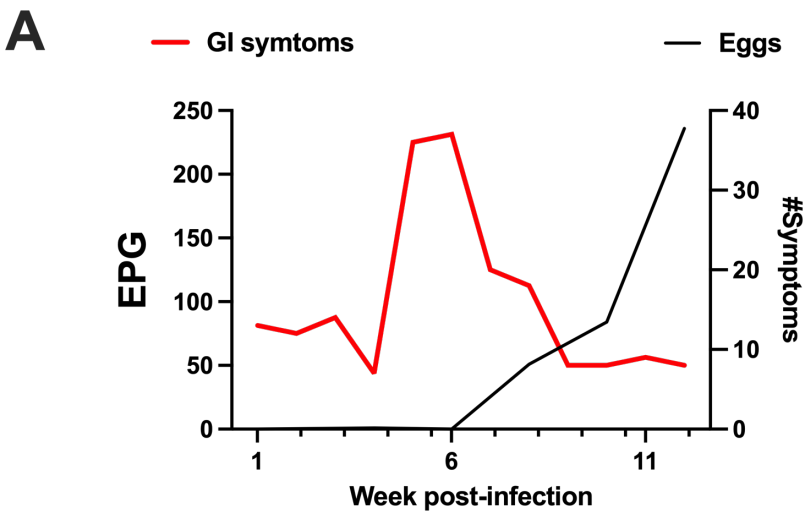

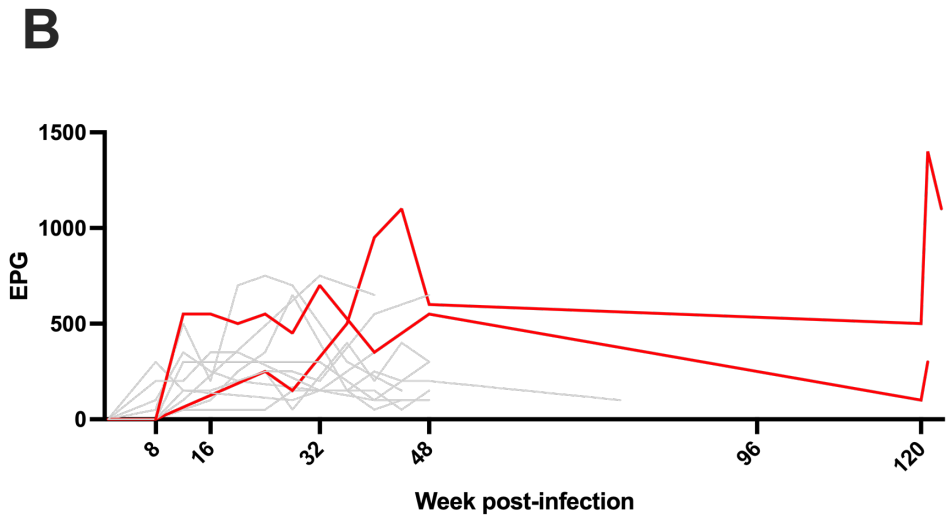

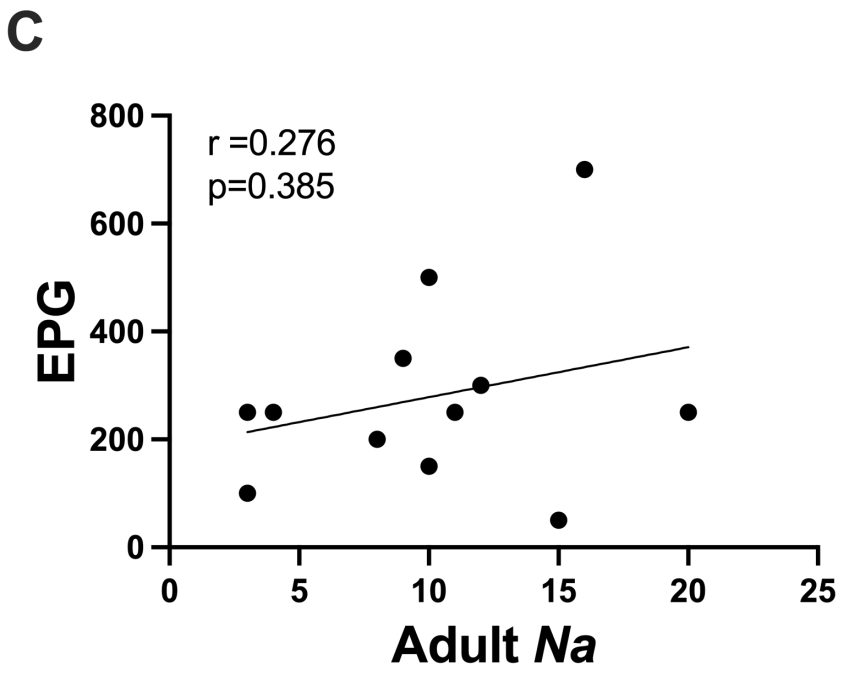

Supplementary Figure 1: Skin reaction, egg counts and adult worm enumeration

(A) GI symptoms (shown in Fig. 2B) plotted against mean egg count. (B) Egg counts highlighting 2 participants (red lines) with patent infection over 120-week post-infection. (C) Correlation between EPG and adult *N. americanus* visualised in the intestine.

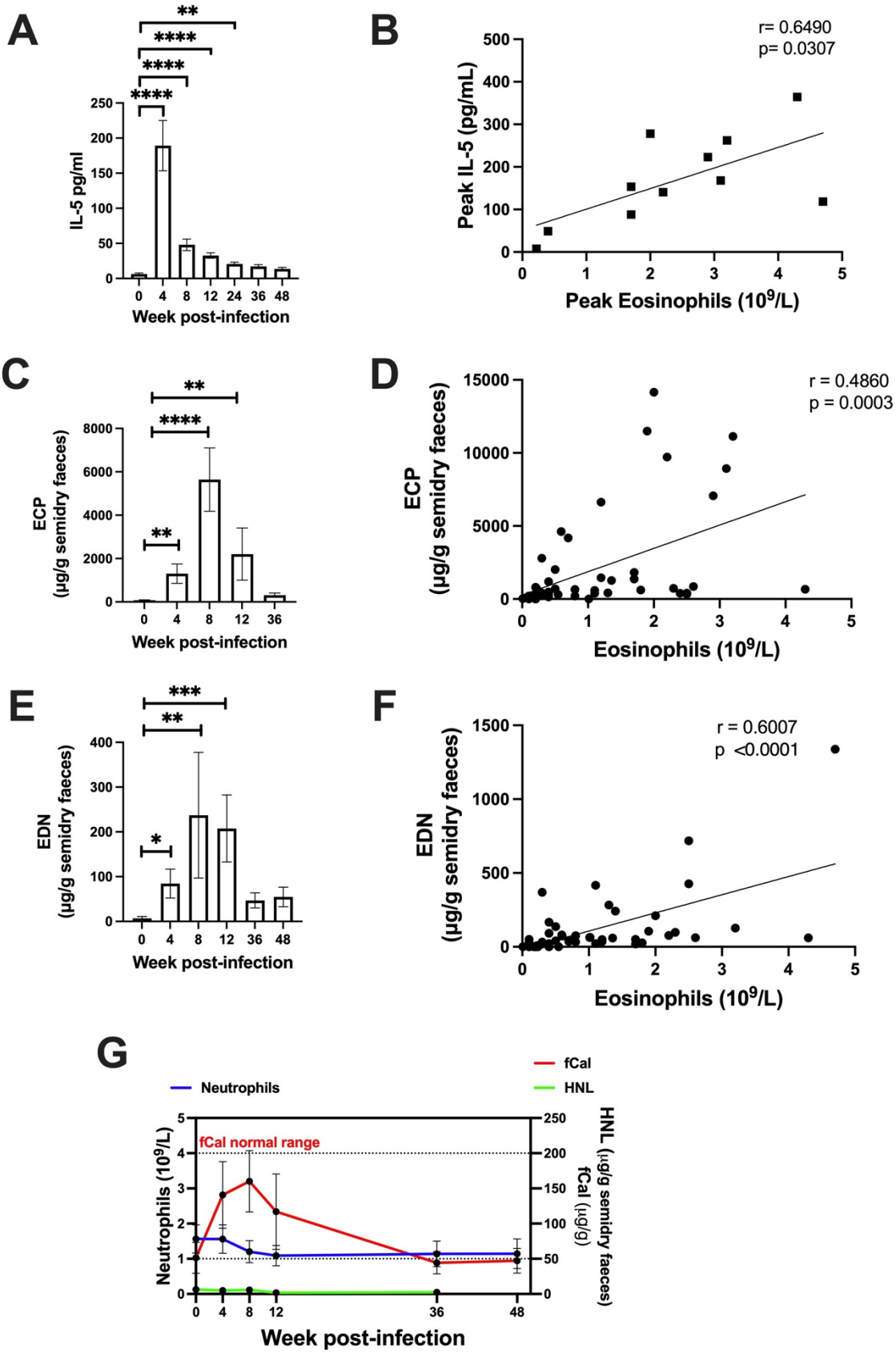

Figure 3: Hookworm infection increases serum IL-5 and faecal eosinophil-specific degranulation markers

(A) Bar graph showing serum IL-5 mean ± SEM. (B) Scatter plot showing correlation between peak serum IL-5 (week 4) and peak eosinophils count (week 8). (C) Bar graph showing ECP mean ± SEM measured in faeces. (D) Correlation between ECP levels and eosinophils count over the course of infection. (E) Bar graph showing EDN mean ± SEM measured in faecal samples. (F) Correlation between EDN levels and eosinophils count over the course of infection. (G) Faecal calprotectin (fCal – red line) plotted against neutrophils count (blue line) and HNL (green line). Showing mean ± SEM. (A) Analysed with One-way ANOVA using Friedman test with Dunn's multiple comparison test. (B, D and F) Analysed with Pearson correlation. (C and E) Analysed using One-way ANOVA using Kruskal-Wallis with Dunn's multiple comparison test. p=*<0.05,**<0.005,***<0.001,****<0.0001.

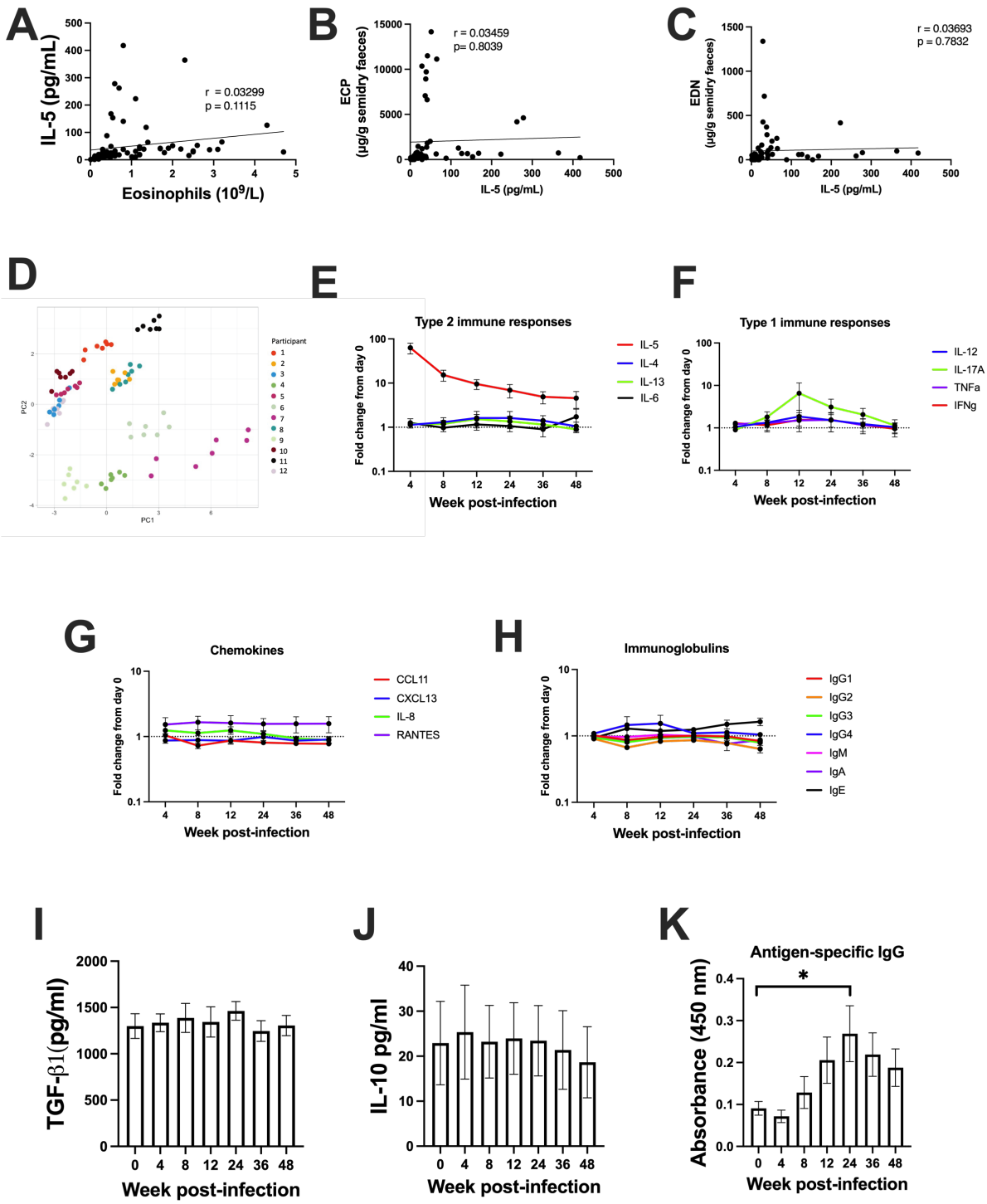

Supplementary Figure 2: Cytokine panels during hookworm infection

IL-5 correlation with (A) eosinophils, (B) ECP, (C) EDN during Na infection. (D) PCA plot created with R software to visualise Luminex data for cytokines and chemokines analysed during the trial. (E-H) Graph showing fold changes from baseline (day 0 – uninfected) of type 2 cytokines (E), type 1 cytokines (F), chemokines (G) and antibodies (H) over the course of infection. (I) Graph showing mean ± SEM of TGF-β1 measured by Luminex (N=8). (J) Mean ± SEM of IL-10 measured in serum by Luminex (N=7). (K) Bar graph showing mean ± SEM of antigen-specific IgG, measured by antigen-specific ELISA.

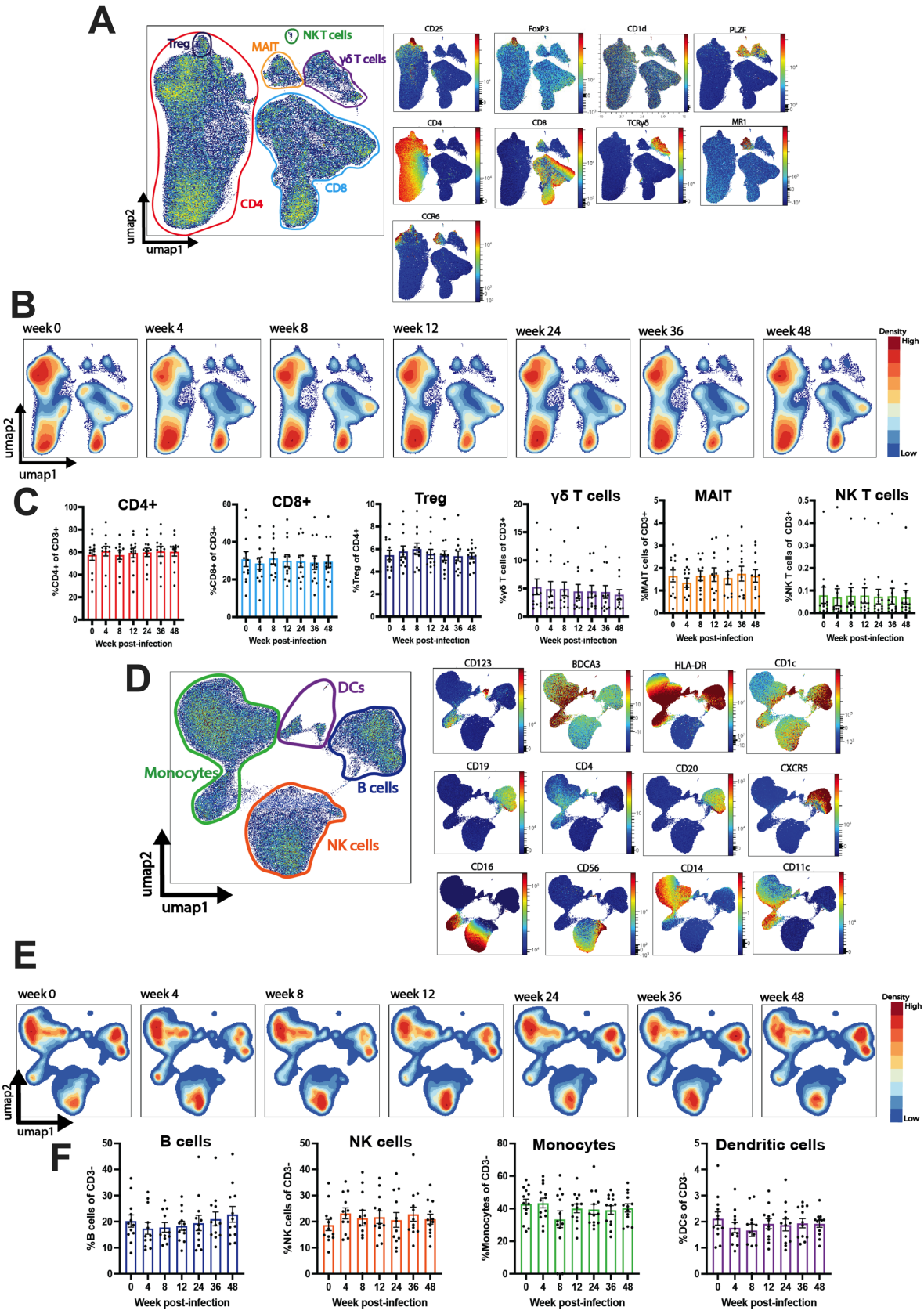

Figure 4: Peripheral blood immune cells are unchanged following *N. americanus* infection

(A)Panel 1 UMAPs identifying main populations and representative marker expression. (B) Panel 1 UMAPs showing population density over the course of infection. (C) Bar graphs showing individual values and mean ± SEM for immune cell population over time. (D) Panel 2 UMAPs identifying main populations and representative marker expression. (E) UMAPs showing population density over the course of infection. (F) Bar graphs showing individual values and mean ± SEM for immune cell population over time for panel 2.

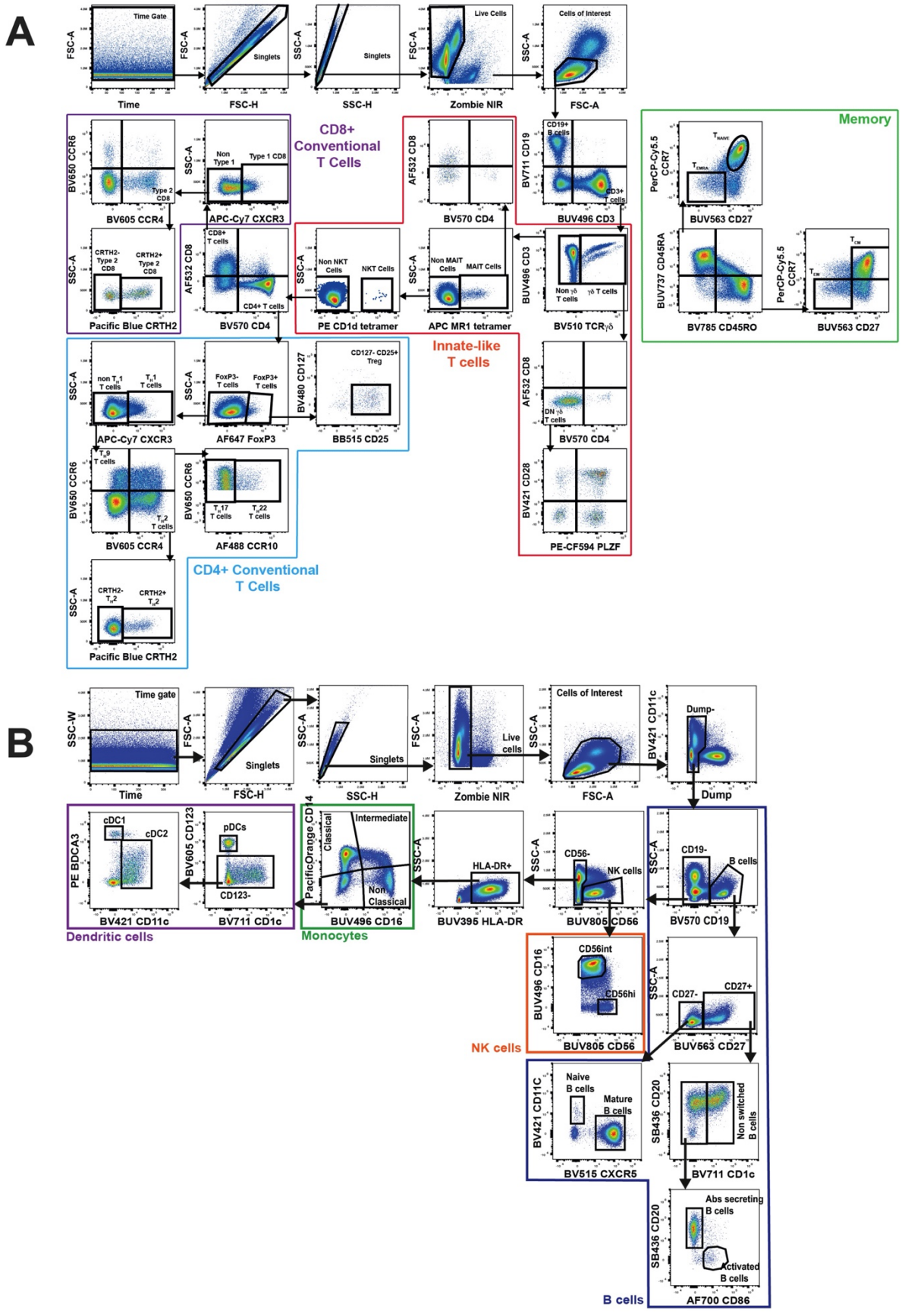

Supplementary Figure 3: PBMCs gating strategies

(A) Gating strategies for PBMCs panel 1. (B) Gating strategies for PBMCs panel 2.

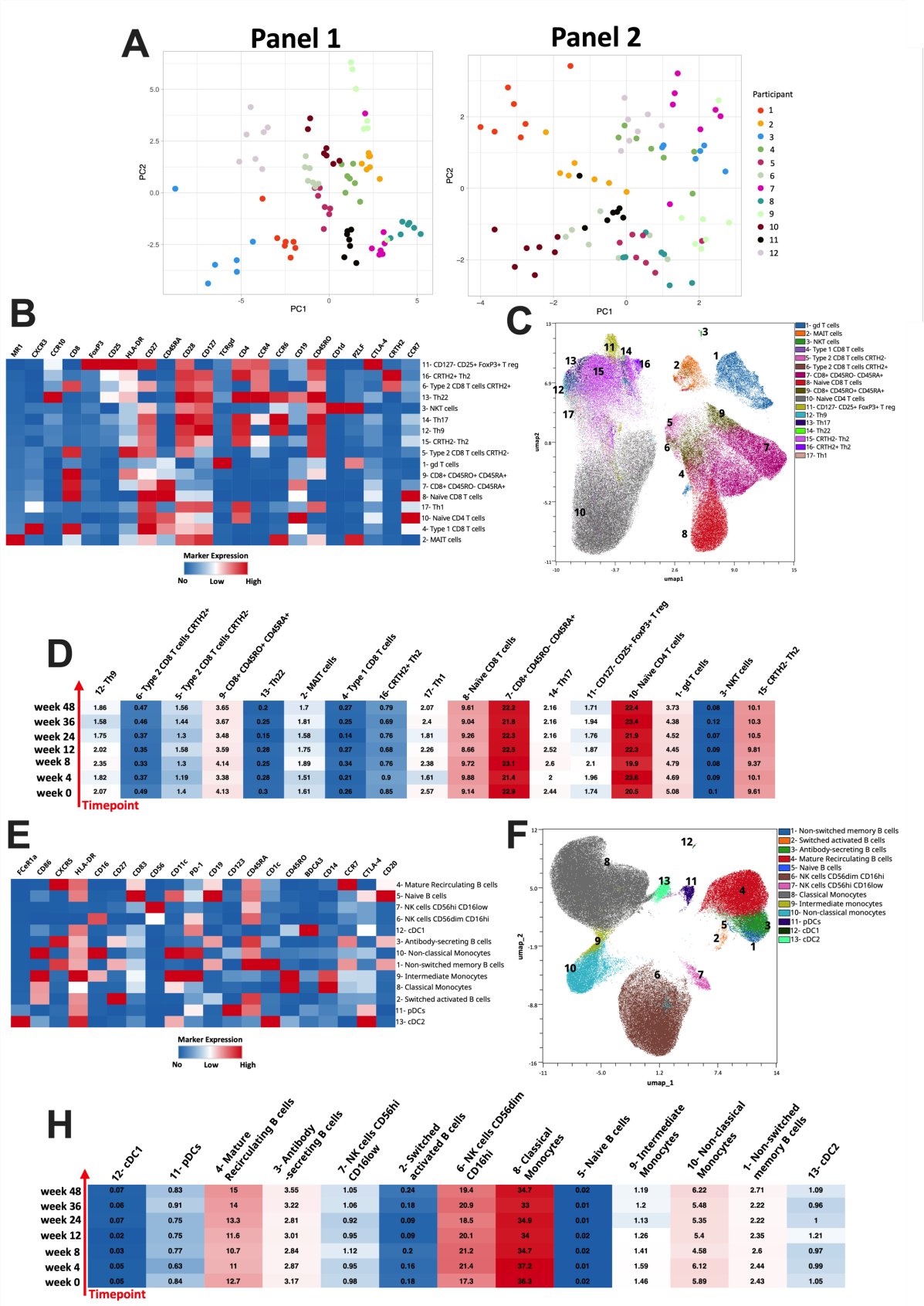

Supplementary Figure 4: PBMC subpopulations unchanged during hookworm infection

(A) Immune cells variability visualized by PCA plot generated using R software.

(B) Heat map summary of median expression values of cell markers expressed by subpopulations identified with panel 1. (C) UMAP generated using OMIQ with overlapped panel 1 subpopulations. (D) Frequencies of subpopulations per timepoints. (E) Heat map summary of median expression values of cell markers expressed by subpopulations identified with panel 2. (F) UMAP generated using OMIQ with overlapped panel 2 subpopulations. (H) Frequencies of subpopulations per timepoints. In (D) and (H) color gradient represent the percentage of population, with red showing the highest and blue the lowest.

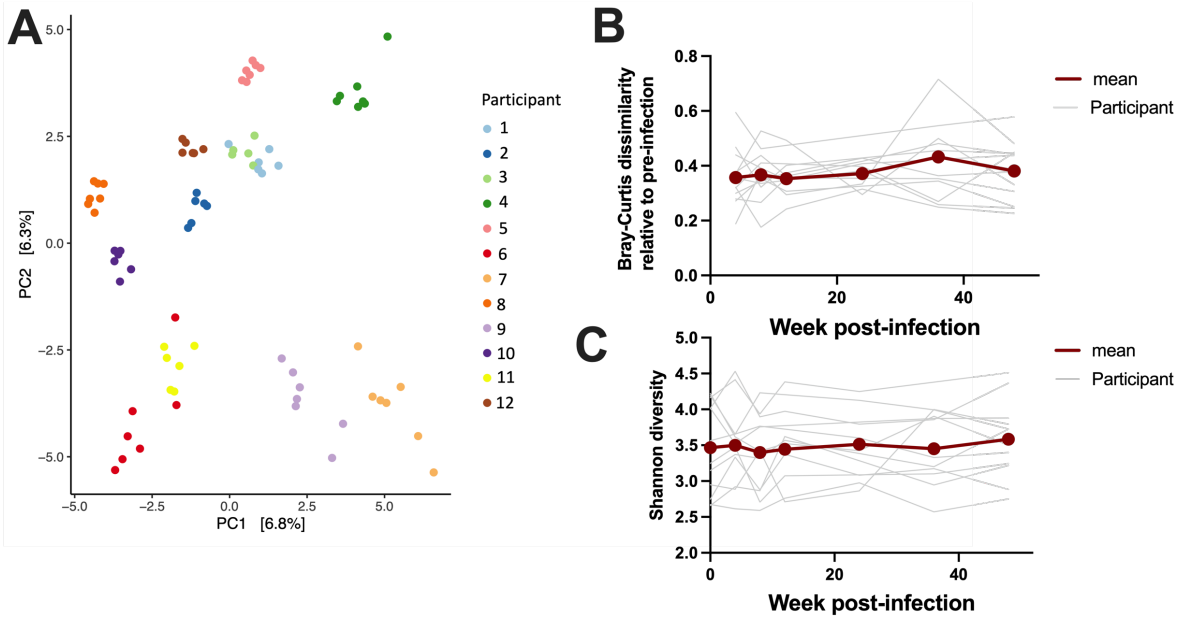

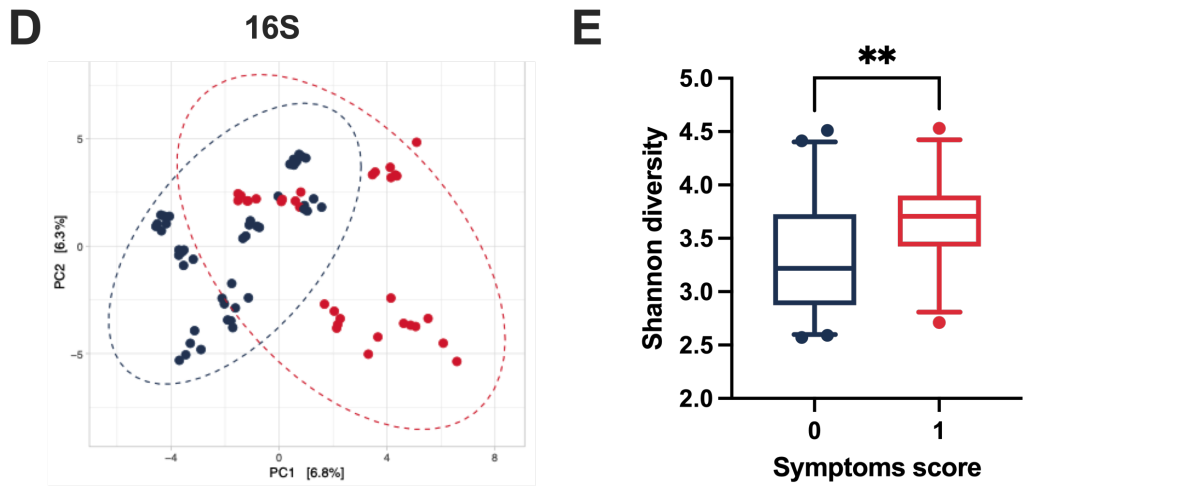

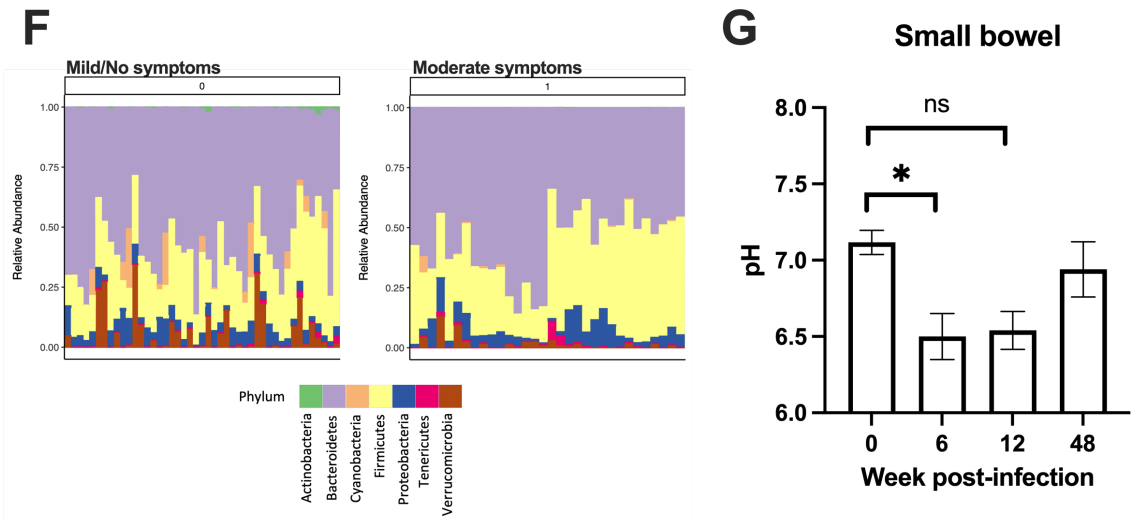

Figure 5: Microbiome stability and small bowel pH during hookworm infection

(A) PCA plots showing individual participants (B) Graph showing Bray-Curtis dissimilarity test for each single participant (grey lines) and mean (dark red line). (C) Shannon diversity showing each participant (grey lines) and mean (dark red line). (D) PCA plot showing 16s analysis grouping participants according to symptoms score (no/mild symptoms (dark blue); moderate symptoms(red)). (E) Box plot showing Shannon diversity accordingly to symptoms (score 0= no/mild symptoms (dark blue); 1= moderate symptoms(red)). (F) Phylum relative abundance for participants with mild/no symptoms (0) and moderate symptoms (1). (G) Small bowel pH measured by Smartpill. Showing mean ± SEM (N=6). (E) Analysed using unpaired t-test **=0.008. (G) Analysed using Wilcoxon t-test *=0.0312.

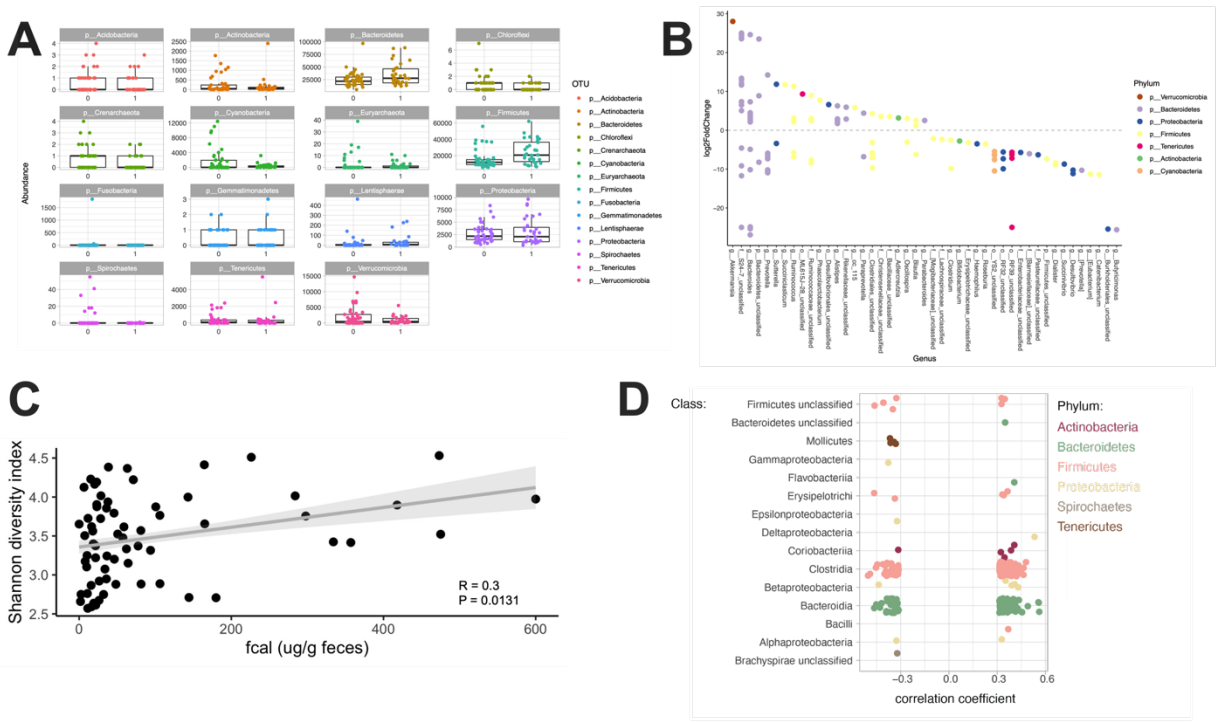

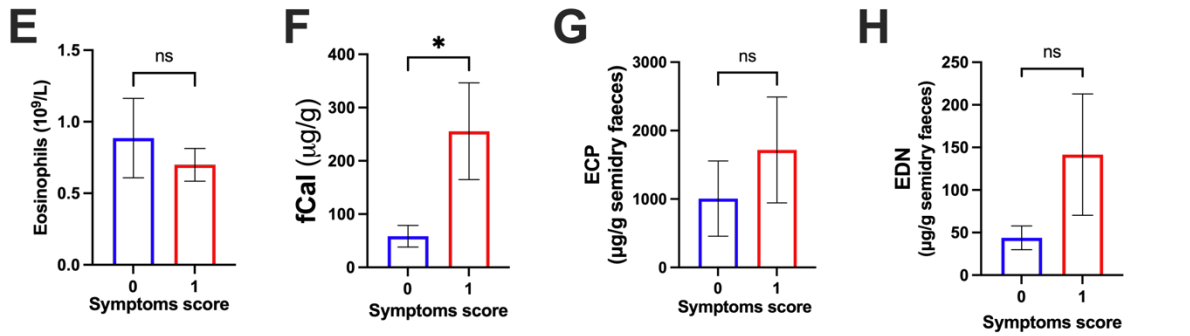

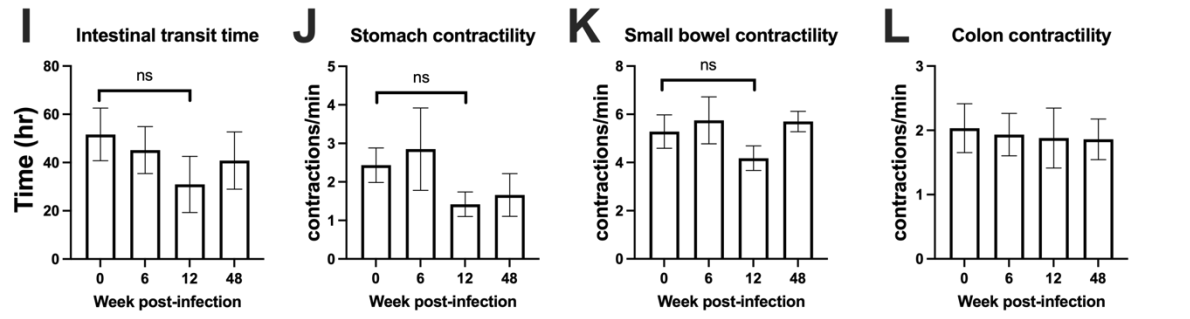

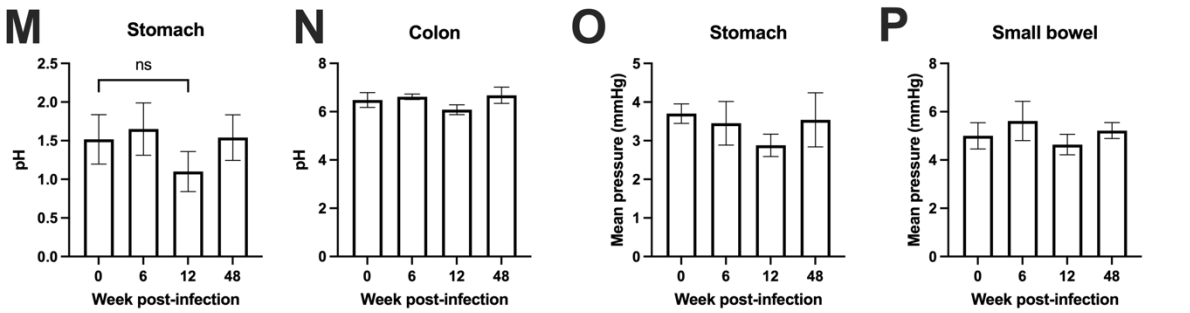

Supplementary Figure 5: Changes in microbiome are associated with moderate symptomology after hookworm infection without changes in gut physiology

(A) Relative abundance of the top 100 most abundant taxa split by those who experience mild to moderate symptoms (symptom score 0) and those who experience severe symptoms (symptom score 1) and faceted by Phylum. (B) OTUs that were identified to be significantly different between those who experience mild to moderate symptoms (symptom score 0) and those who experience severe symptoms (symptom score 1) as determined using DESeq2 with an adjusted P value < 0.01. (C) Spearman correlation between an individual's microbiome diversity (Shannon index) and fCal levels. (D) OTUs that were identified to have a significant Spearman correlation (P < 0.01) with fecal calprotectin levels. Correlation coefficient is plotted and OTUs are arranged by Class. Color represents Phylum. (E-H) Mean ± SEM of eosinophils count (E), fCal (F), ECP (G) and EDN (H) according to symptoms score. (I-P) Gut physiology measured through Smartpill^{TM} (N=6), bar graph showing mean ± SEM for intestinal transit time (I), stomach contractility (J), small bowel contractility (K) and colon contractility (L). Changes in pH in the stomach (M) and colon (N). Mean pressure in the stomach (O) and small bowel (P). (E-H) Analysed using Mann-Whitney t-test, (I-P) analysed using one-way ANOVA with Kruskal-Wallis multiple comparison test. *<0.05

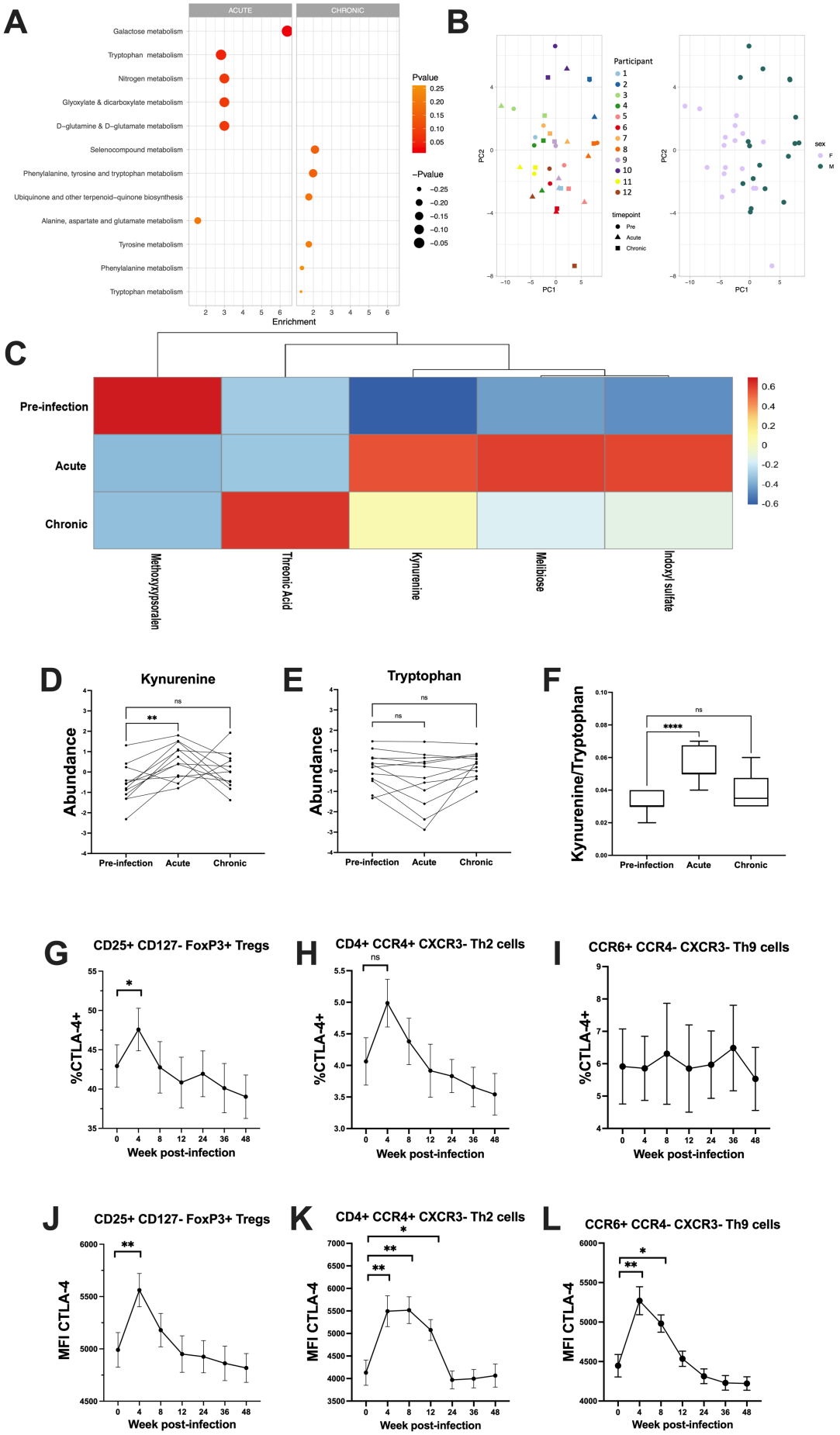

Figure 6: Changes in the plasma metabolome over the course of hookworm infection

(A) Top six enriched metabolic pathways identified using MSEA comparing pre-infection vs acute phase (left panel) or chronic phase of infection (right panel). (B) PCA scores plot on the plasma polar metabolome labelled by participant and by sex. (C) Heatmap of five annotated plasma metabolites significantly ($p < 0.05$) changed over the course of hookworm infection, as determined by mixed-mode, two-way analysis of variance (ANOVA), controlling for 'Participant ID' and 'sex' as covariates. (D) Post-hoc analysis indicating changes in plasma kynurenine levels over the course of hookworm infection. significantly different to pre-infection kynurenine levels by Dunnett's post-hoc test. (E) Changes in plasma tryptophan levels over the course of hookworm infection. (F) Changes in plasma kynurenine/tryptophan ratio, a marker of indoleamine 2,3-dioxygenase (IDO) activity. Frequency of CTLA-4+ (G) CD25+ CD127- FoxP3+ T_{REG}, (H) CD4+ CCR4+ CXCR3- T_H2 cells and (I) CCR6+ CCR4- CXCR3- T_H9 cells. (J-L) CTLA-4 MFI for population showed in G-H-I respectively. Graphs showing mean± SEM. In (D-F) values shown in the graph represent log_{10} transformed, auto scaled normalized data (N = 12 participants). Results were analysed with (F-G) Dunnett's post-hoc test, (G-N) One-way ANOVA with Mixed-effect analysis with Tukey's multiple comparison test. p= *<0.05, **<0.005, ***< 0.0005, ****<0.0001

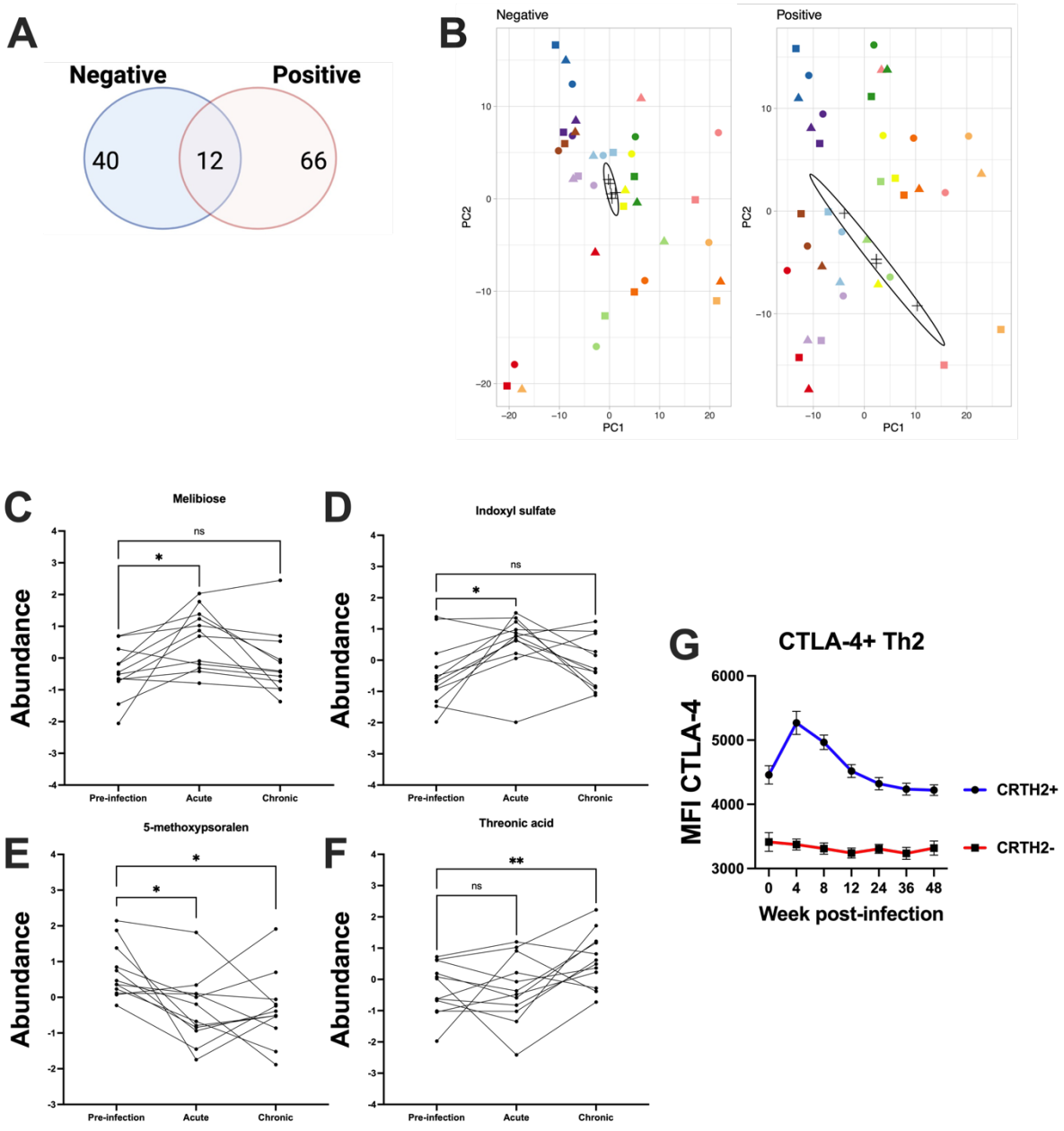

Supplementary Figure 6: Changes in polar metabolites and CTLA-4 expression

(A) Number of annotated plasma metabolites detected in the negative or positive electrospray ionization (ESI) modes, including those detected in both modes. (B) Data overview and quality assurance demonstrating good method reproducibility in the negative (left panel) and positive ESI (right panel) modes, as reflected by tight clustering of QCs evident in the principal component analysis (PCA) scores plots. Changes in plasma levels of (C) Melibiose, (D) indoxyl sulphate, (E) 6-Methoxypsoralen, or (F) threonic acid, over the course of hookworm infection.*$p< 0.05$; **$p < 0.01$, significantly different to pre-infection kynurenine levels by Dunnett's post-hoc test, following Mixed ANOVA analysis. Values shown represent log_{10} transformed, auto scaled normalized data (N = 12 participants). (G) Graph showing expression of CTLA-4 (MFI) for CRTH2+ (blue) and CRTH2- (red) CD4+ CCR4+ CXCR3- T_H2 cells. Values shown are mean± SEM (N = 12 participants).

Data File S1

Participant Inclusion Criteria

- Participant has provided written informed consent and is willing to comply with all Protocol scheduled visits, laboratory tests, and other trial procedures and in the opinion of the Investigator has a good understanding of the Protocol, the length of the study and the demands of the study.
- Participants will be male and non-pregnant, non-lactating females aged between 18 to 65 years.
- Participants must weigh more than 50kg with a BMI within the 18 – 35kg/m^2 range
- Participants must understand the procedures involved and agree to participate in the study by giving fully informed, written consent prior to any study assessment.
- Participants must be contactable and available for the duration of the clinical trial.
- If female, has met either of criterion "a or "b" below:
  (a) If of non-childbearing potential, has met 1 of the following – Amenorrhoeic for at least 2 years, or has had a hysterectomy and/or bilateral oophorectomy at least 8 weeks prior to screening, or has had a tubal ligation at least 8 weeks prior to screening.
  (b) If of childbearing potential, must be willing to use the acceptable methods of contraception
- In the opinion of the investigator is in good general health

Participant Exclusion Criteria

- Current or history of helminth infection (other than *E. vermicularis*).
- Have any finding at screening that in the opinion of the Investigator or medical monitor would compromise the safety of the Participant or affect their ability to adhere to protocol scheduled visits, treatment plan, laboratory tests, and other trial procedures.
- Have participated in any other clinical trial and/or have received an investigational drug or device within 30 days of screening.
- History or current evidence of any of the following: compromised respiratory function (chronic obstructive pulmonary disease, respiratory depression, signs or symptoms of hypoxia at screening); thyroid pathology (unless stabilized and euthyroid for >3 months at the time of screening); hepatitis B, hepatitis C, or human immunodeficiency virus (HIV) infection; evidence of clinically significant chronic cardiac, hepatic or renal disease; psychiatric illness (poorly controlled); seizure disorder or any other chronic health issues that in the opinion of the Investigator would exclude the Participant from the trial.
- Have one of the following laboratory abnormalities: ferritin <20 □g/L, transferrin <2.04 g/L or Hb <120 g/L for females or 130 g/L for males.
- History of severe asthma or other health conditions that may require future steroid use;
- History of substance abuse or current substance abuse that in the opinion of the Investigator would exclude the Participant from the trial.
- History of intolerance, allergy or hypersensitivity to the proposed anthelmintic – mebendazole.
- History of intolerance, allergy or hypersensitivity to the Betadine (iodine) solution used in preparation of *N. americanus* that in the opinion of the Investigator would exclude the participant from the trial.
- History of malignancy of any organ system (other than localized basal cell carcinoma of the skin), treated or untreated, within the past 5 years;
- For female subjects: positive urine pregnancy test at screening.

- Current or past scars, tattoos, or other disruptions of skin integrity at the intended site of larval application.
- Poor venous access making the Participant unable to comply with the safety laboratory testing requirements.
- Probiotic or prebiotic supplementation within 1 month of screening or commencement during the study
- Laxative or gastric motility medication use within 1 month of screening or commencement during the study
- Significant dietary change or weight loss (>5%) within 6 months of screening or during the study
- Smokers or high alcohol consumers

Data File S2 : List of flow cytometry antibodies

Whole Blood Antibodies

Antigen	Fluorophore	Clone	#Cat	Supplier
CD19	BUV805	HIB19	742007	BD
FceRIa	BV421	AER-37 (CRA-1)	334624	Biolegend
CD10	BV480	HI10a	746847	BD
CD56	BV570	HCD56	318330	Biolegend
CD123	BV605	6H6	306026	Biolegend
CD11b	BV650	ICRF44	301336	Biolegend
CD15s	BV711	CSLEX1	563910	BD
CD4	BV750	SK3	344644	Biolegend
Siglec8	BV786	837535	747868	BD
HLADR	FITC	G46-6	307604	Biolegend
CD3	AF532	UCHT1	58-0038-42	Thermofisher
CD16	PerCP	3G8	302030	Biolegend
CXCR4 (CD184)	PE-CF594	12G5	562389	BD
CD8	PE-Cy5	RPA-T8	301010	Biolegend
CD203c	APC	NP4D6	324610	Biolegend
CD14	AF700	HCD14	325614	Biolegend
CD15	APC-Cy7	W6D3	323048	Biolegend

PBMC Antibodies

Antigen	Fluorophore	Clone	#Cat	Supplier
CCR10	AF488		RDSFAB3478G0100	R&D Systems
CD11c	BV421	3.9	301628	Biolegend
CD123	BV605	6H6	306026	Biolegend
CD127	BV480	HIL-7R-M21	566101	BD Biosciences
CD14	PacOrange	TuK4	MHCD1430	ThermoFisher
CD141 (BDCA3)	PE	AD5-14H12	130-113-318	Miltenyi Biotec
CD15	PE-Cy7	W6D3	323030	Biolegend
CD16	BUV496	3G8	612944	BD Biosciences
CD183 (CXCR3)	APC-Cy7	G025H7	353722	Biolegend
CD185 (CXCR5)	BB515	RF8B2	564624	BD Biosciences
CD19	BV570	HIB19	302236	Biolegend
CD19	BV711	Sj25C1	563036	BD Biosciences
CD194 (CCR4)	BV605	L291H4	359418	Biolegend
CD196 (CCR6)	BV650	11A9	563922	BD Biosciences
CD197 (CCR7)	PerCP-Cy5.5	G043H7	353220	Biolegend
CD1c	BV711	L161	331536	Biolegend

CD20	SB436	2H7	62-0209-42	ThermoFisher
CD203c	PE-Cy7	NP4D6	324618	Biolegend
CD25	APC-Fire750	BC96	302642	Biolegend
CD25	BB515	2A3	564467	BD Biosciences
CD27	BUV563	M-T271	741336	BD Biosciences
CD279 (PD-1)	BV480	EH12.1	566112	BD Biosciences
CD28	BV421	CD28.2	302930	Biolegend
CD294 (CRTH2)	PacBlue	BM16	350130	Biolegend
CD3	BUV496	UCHT1	612940	BD Biosciences
CD3	PE-Cy7	UCHT1	300420	Biolegend
CD4	AF532	RPA-T4	58-0049-42	ThermoFisher
CD4	BV570	RPA-T4	300534	Biolegend
CD45RA	BUV737	HI100	612846	BD Biosciences
CD45RA	BV650	HI100	304136	Biolegend
CD45RO	BV785	UCHL1	304234	Biolegend
CD56	BUV805	NCAM16.2	749086	BD Biosciences
CD8	AF532	RPA-T8	58-0088-42	ThermoFisher
CD80	BV510	2D10	305234	Biolegend
CD83	BUV737	HB15E	612823	BD Biosciences
CD86	AF700	FUN-1	561124	BD Biosciences
CTLA-4	PE-Cy7	14D3	25-1529-42	ThermoFisher
CTLA-4	PerCP-eFluor710	14D3	46-1529-42	ThermoFisher
FceR1a	AF647	AER-37	334614	Biolegend
FoxP3	AF647	259D	320214	Biolegend
HLA-DR	BUV395	G46-6	564040	BD Biosciences
PLZF	PE-CF594	R17-809	565738	BD Biosciences
TCRgd	BV510	B1	331220	Biolegend
CD1d Tetramer	PE	BS-57	53235	NIH Tetramer Core Facility
MRI Tetramer	APC	5-OP-RU	53233	NIH Tetramer Core Facility
Zombie NIR Viability Dye				Biolegend

Data File S4. Accurate masses and retention times of all annotated metabolites detected in plasma analyzed using negative and positive electrospray ionization modes.

No	Plasma metabolite	Mode	Adduct type	Average Rt(min)	Average m/z	Reference m/z	Formula	Ontology	INCHIKEY	SMILES
1	Gentiobiose	Positive	[M+Na]+	10.516	365.1051	365.10544	C12H22O11	O-glycosyl compounds	DLRVVLDZNNYCBX-CQUJWQHSSA-N	OCC1OC(OCC2OC(O)C(O)C(O)C2O)C(O)C(O)C1O
2	(1R,2R,5R,5'S,6S,8aS)-6-(acetyloxy)-2,5,8a-trimethyl-5''-oxo-octahydro-2H-dispiro[naphthalene-1,2':5',3''-bis(oxolane)]-5-ylmethyl acetate	Positive	[M+Na]+	5.684	459.24881	459.23999	C24H36O7	Diterpene lactones	JZNGEGWFNPRYBH-URQJKXJZSA-N	O=C(OCC1(C)C(OC(=O)C)CCC2(C)C1CCC(C)C32OC4(COC(=O)C4)CC3)C
3	(2R)-6-methylpiperidine-2-carboxylic acid	Positive	[M+H]+	6.137	144.1017	144.10001	C7H13NO2	L-alpha-amino acids	IHLDCUQUFBWSJU-PRJDIBJQSA-N	O=C(O)C1NC(C)CCC1
4	(5E)-6,10-dimethyl-5,9-undecadien-2-one	Positive	[M+Na]+	9.083	217.15379	217.16	C13H22O	Acyclic monoterpenoids	HNZUNIKWNYHEJJ-FMIVXFBMSA-N	O=C(C)CC=C(C)CCC=C(C)C
5	1-Lauroyl-2-hydroxy-sn-glycero-3-phosphocholine	Positive	[M+H]+	5.927	440.27679	440.27716	C20H42NO7P	1-acyl-sn-glycero-3-phosphocholines	BWKILASWCLJPBO-LJQANCHMSA-N	CCCCCCCCCCCC(=O)OC[C@@H](O)COP([O-])(=O)OCC[N+](C)(C)C
6	1,3-Dimethylurate	Negative	[M+H]-	3.478	195.05161	195.05237	C7H8N4O3	Xanthines	OTSBKHHWSQYEHK-UHFFFAOYSA-N	CN1C2=C(N=C(O)N2)C(=O)N(C)C1=O
7	2-Hydroxyvaleric acid	Negative	[M-H]-	5.438	117.0554	117.05572	C5H10O3	Hydroxy fatty acids	JRHWHSJDIILJAT-UHFFFAOYNA-N	CCCC(O)C(O)=O
8	2-Phenylacetamide	Positive	[M+H]+	9.017	136.0752	136.07568	C8H9NO	Phenylacetamides	LSBDFXRDZJMBSC-UHFFFAOYSA-N	N=C(O)CC=1C=CC=CC1
9	3-carboxy-4-methyl-5-propyl-2-furanpropanoic acid	Negative	[M-H]-	4.426	239.0929	239.0925	C12H16O5	Furanoid fatty acids	WMCQWXZMVIETAO-UHFFFAOYSA-N	O=C(O)C1=C(OC(=C1C)CCC)CCC(=O)O
10	3-Formylindole	Positive	[M+H]+	7.92	146.05969	146.06004	C9H7NO	Indoles	OLNJUISKUQQNIM-UHFFFAOYSA-N	O=CC1=CNC2=CC=CC=C12
11	3-hydroxy-1,2-dimethylpyridin-4(1H)-one	Positive	[M+H]+	6.413	140.06779	140.07001	C7H9NO2	Methylpyridines	TZXKOCQBRNJULO-UHFFFAOYSA-N	O=C1C=CN(C(=C1O)C)C
12	3-Hydroxyanthranilic acid	Positive	[M+H]+	9.321	154.0583	154.04988	C7H7NO3	Hydroxybenzoic acid derivatives	WJXSWCUQABXPFS-UHFFFAOYSA-N	c1cc(c(c(c1)O)N)C(=O)O
13	3-Hydroxypyridine	Negative	[M-H]-	7.907	94.0293	94.02984	C5H5NO	Hydroxypyridines	GRFNBEZIAWKNCO-UHFFFAOYSA-N	OC1=CN=CC=C1
14	3-Indoxyl sulfate	Negative	[M-H]-	10.982	212.0023	212.0023	C8H7NO4S	Arylsulfates	BXFFHSIDQOFMLE-UHFFFAOYSA-N	OS(=O)(=O)OC1=CNC2=CC=CC=C12
15	4-Hydroxybenzoate	Negative	[M-H]-	9.613	137.02431	137.024	C7H6O3	Hydroxybenzoic acid derivatives	FJKROLUGYXJWQN-UHFFFAOYSA-N	O=C(O)C1=CC=C(O)C=C1
16	4-Hydroxybenzoylcholine	Positive	[M]+	6.719	224.1282	224.12756	C12H18NO3	Benzoic acid esters	BAPAICNRGIBFJT-UHFFFAOYSA-O	C[N+](C)(C)CCOC(O)=C1C=CC(=O)C=C1
17	4-Hydroxymandelonitrile	Positive	[M+H]+	10.305	150.05161	150.05496	C8H7NO2	1-hydroxy-2-unsubstituted benzenoids	HOOOPXDSCKBLFG-UHFFFAOYNA-N	N#CC(O)C1=CC=C(O)C=C1
18	4-Pyridoxate	Negative	[M-H]-	8.72	182.04601	182.04588	C8H9NO4	Pyridinecarboxylic acids	HXACOUQIXZGNBF-UHFFFAOYSA-N	CC1=C(O)C(C(O)=O)=C(CO)C=N1
19	5-Methoxypsoralen	Negative	[M-H]-	7.345	215.03259	215.03499	C12H8O4	5-methoxypsoralens	BGEBZHIAGXMEMV-UHFFFAOYSA-N	O=C1OC=2C=C3OC=CC3=C(OC)C2C=C1
20	5-Methylcytosine	Negative	[M+H]+	10.29	126.0622	126.06618	C5H7N3O	Hydroxypyrimidines	LRSASMSXMSNRBT-UHFFFAOYSA-N	CC1=CN=C(O)NC1=N
21	Acetylcamitine	Positive	[M]+	2.948	204.1228	204.12248	C9H18NO4	Acyl camitines	RDHQFKQIGNGIED-UHFFFAOYNA-O	O=C(OC(CC[=O)O)C[N+](C)(C)C)C
22	Alanine	Positive	[M+H]+	9.792	90.0546	90.05495	C3H7NO2	Alanine and derivatives	QNAYBMKLOCPYGJ-UHFFFAOYNA-N	CC(N)C(O)=O
23	Arginine	Positive	[M+H]+	9.046	175.11861	175.119	C6H14N4O2	Arginine and derivatives	ODKSFYDXXFIFQN-UHFFFAOYSA-N	O=C(O)C(N)CCCN=C(N)N
24	Asparagine	Positive	[M+H]+	10.794	133.06039	133.06078	C4H8N2O3	Asparagine and derivatives	DCXYFEDJOCDNAF-UHFFFAOYNA-N	NC(CC(=O)=N)C(O)=O
25	Atractylenolide II	Positive	[M+Na]+	9.036	255.1369	255.13	C15H20O2	Eudesmanolides, and derivatives	OQYBLUDOOFOBPO-KCQAQPDRSA-N	O=C1OC2C(=C1C)CC3C(=C)CCCC3(C)C2
26	aurapten	Negative	[M-H]-	6.909	297.15329	297.1496	C19H22O3	Terpene lactones	RSDDHGSKLOSQFK-RVDMUPIBSA-N	O=C1OC=2C=C(OCC=C(C)CCC=C(C)C)C=CC2C=C1
27	Azelaic acid	Negative	[M-H]-	3.376	187.09801	187.09758	C9H16O4	Medium-chain fatty acids	BDJRBEYXGGNYIS-UHFFFAOYSA-N	O=C(O)CCCCCCCC(=O)O
28	Bilirubin	Negative	[M-H]-	2.668	583.25677	583.25623	C33H36N4O6	Bilirubins	BPYKTIZUTYGOLE-IFADSCNNSA-N	O=C(O)CCC1=C(NC(C=C2N=C(O)C(=C2C=C)C)=C1C)CC=3NC(C=C4N=C(O)C(C=C)=C4C)=C(C3CCC(=O)O)C
29	Biliverdin	Negative	[M+H]+	5.943	583.25458	583.25513	C33H34N4O6	Bilirubins	QBUVFDKTZJNUPP-UHFFFAOYSA-N	O=C(O)CCC=1C(N=C(C=C2N=C(O)C(C=C)=C2C)C1C)=CC=3NC(C=C4N=C(O)C(=C4C=C)C)=C(C3CCC(=O)O)C
30	Butyryl carnitine	Positive	[M+H]+	1.494	232.1543	232.1553	C11H21NO4	Acyl camitines	LRCNOZRCYBNMEP-UHFFFAOYNA-N	O=C([O-])CC(OC(=O)CCC)C[N+](C)(C)C
31	Caffeine	Positive	[M+H]+	0.761	195.0871	195.08765	C8H10N4O2	Xanthines	RYYVLZVUVIJVGH-UHFFFAOYSA-N	CN1C=NC2=C1C(=O)N(C)C(=O)N2C
32	Camitine	Positive	[M]+	6.529	162.1125	162.11247	C7H15NO3	Camitines	PHIQHXFUZVPYII-ZCFIWIBFSA-N	C[N+](C)(C)CC(O)CC([O-])=O
33	Chlorothalonil-4-hydroxy	Negative	[M-H]-	4.669	244.9079	244.90817	C8HCl3N2O	Benzonitriles	MDQKYGOECVSPIW-UHFFFAOYSA-N	C(Cl)=C(C(#N)=C(Cl)C(=C(Cl)Cl)O)Cl)#N
34	Cholesterol	Positive	[M+H-H2O]-	0.716	369.3515	369.35199	C27H46O	Cholesterols and derivatives	HVYWMOMLDIMFJA-UHFFFAOYSA-N	OC1CC2=CCC3(CCC4(C)C(CCC34)C(C)CCCC(C)C)C2(C)CC1
35	Choline	Positive	[M]+	10.823	104.1062	104.10645	C5H14NO	Cholines	OEYIOHPDSNJKLS-UHFFFAOYSA-N	C[N+](C)(C)CCO
36	Citrulline	Positive	[M+H]+	11.293	176.1026	176.10297	C6H13N3O3	L-alpha-amino acids	RHGKLRLOHDJJDR-BYPYZUCNSA-N	N[C@@H](CCCNC(O)=N)C(O)=O
37	Creatine	Positive	[M+H]+	9.322	132.07651	132.08	C4H9N3O2	Alpha amino acids and derivatives	CVSVTCORWBXHQV-UHFFFAOYSA-N	O=C(O)CN(C)C(=N)N
38	Creatinine	Positive	[M+H]+	2.621	114.0659	114.06618	C4H7N3O	Alpha amino acids and derivatives	DDRJAANPRJIHGJ-UHFFFAOYSA-N	N=C1N=C(O)CN1C
39	Cystine	Positive	[M+H]+	13.333	241.03101	241.03113	C6H12N2O4S2	L-cysteine-S-conjugates	LEVWYRKDKASIDU-UHFFFAOYNA-N	NC(CSSCC(N)C(O)=O)C(O)=O
40	Decanoyl-L-camitine	Positive	[M+H]+	1.422	316.24789	316.24823	C17H33NO4	Acyl camitines	LZOSYCMHQXPBFU-UHFFFAOYSA-N	O=C([O-])CC(OC(=O)CCCCCCCCC)C[N+](C)(C)C
41	Dehydroisoandrosterone sulfate	Negative	[M-H]-	6.869	367.15909	367.15848	C19H28O5S	Sulfated steroids	CZWCKYRVOZZJNM-UHFFFAOYNA-N	O=C1CC2C3CCC4=CC(=O)CCC4(C)C3CCC(OS(=O)(=O)O)C2C4(C)CC1=O
42	Dodecylbenzenesulfonic acid	Negative	[M-H]-	6.547	325.18411	325.1843	C18H30O3S	Benzenesulfonic acids and derivatives	KXWICGTUELOLSQ-UHFFFAOYSA-N	CCCCCCCCCCCC1=CC=C(C=C1)S(O)(=O)=O
43	Ecgonine	Negative	[M+H]+	7.557	186.1116	186.11247	C9H15NO3	Tropane alkaloids	PHMBVCPLDPDESM-UHFFFAOYNA-N	O=C(O)C1C(O)CC2N(C)C1CC2
44	Ectoine	Positive	[M+H]+	8.605	143.08099	143.082	C6H10N2O2		WQXNXVUDBPYKBA-YFKPBYRVSA-N	O=C(O)C1NC(=NCC1)C
45	Ergothioneine	Positive	[M+H]+	9.172	230.09531	230.09578	C9H15N3O2S	Histidine and derivatives	SSISHJJTAXXQAX-UHFFFAOYNA-N	O=C(O)C(CC1=CN=C([S-])N1)[N+](C)(C)C
46	Erucamide	Positive	[M+H]+	0.716	338.34329	338.34174	C22H43NO	Fatty amides	UAUDZVJPLUQNMU-UHFFFAOYSA-N	N=C(O)CCCCCCCCCCC=CCCCCCCCC
47	Glutamine	Positive	[M+H]+	10.581	147.0761	147.07642	C5H10N2O3	Alpha amino acids	ZDXPYRJPNDTMRX-VKHMYHEASA-N	N[C@@H](CCC(O)=N)C(O)=O
48	Glycocholate	Negative	[M-H]-	10.039	464.30191	464.30099	C26H43NO6	Glycinated bile acids and derivatives	RFDAIACWWDREDC-RGWSMLPJSA-N	O=C(O)CNC(=O)CCC(C)C1CCC2C3C(O)CC4CC(O)CCC4(C)C3CC(O)C12C
49	Glycodeoxycholic acid	Positive	[M+Na]+	7.997	472.3038	472.30301	C26H43NO5		WVULKSPCQVQLCU-JKPPYMBGSA-N	O=C(O)CN=C(O)CCC(C)C1CCC2C3CCC4CC(O)CCC4(C)C3CC(O)C12C
50	Glycohyodeoxycholic acid	Negative	[M-H]-	7.941	448.30719	448.30701	C26H43NO5	Glycinated bile acids and derivatives	SPOIYSFQOFYOFZ-BRDORRHWSA-N	O=C(O)CN=C(O)CCC(C)C1CCC2C3CC(O)C4CC(O)CCC4(C)C3CCC12C
51	Hippurate	Negative	[M-H]-	8.492	178.05119	178.05	C9H9NO3	Hippuric acids	QIAFMBKCNZACKA-UHFFFAOYSA-N	O=C(O)CNC(=O)C=1C=CC=CC1
52	Histidine	Positive	[M+H]+	9.799	156.0766	156.07675	C6H9N3O2	Histidine and derivatives	HNDVDQJCIGZPNO-YFKPBYRVSA-N	N[C@@H](CC1=CN=CN1)C(O)=O
53	HydroxyButyric acid	Negative	[M-H]-	6.83	103.0398	103.04007	C4H8O3	Alpha hydroxy acids and derivatives	AFENDNXGAFYKQO-VKHMYHEASA-N	CC[C@H](O)C(O)=O
54	Hypoxanthine	Positive	[M+H]+	4.304	137.04559	137.04579	C5H4N4O	Hypoxanthines	FDGQSTZJBFJUBT-UHFFFAOYSA-N	OC1=NC=NC=2NC=NC12
55	Indolelactic acid	Negative	[M-H]-	7.846	204.0659	204.06662	C11H11NO3	Indolyl carboxylic acids and derivatives	XGILAAMKEQUXLS-UHFFFAOYNA-N	O=C(O)C(O)CC1=CNC=2C=CC=CC21
56	Isoleucine	Positive	[M+H]+	7.76	132.1021	132.10191	C6H13NO2	L-alpha-amino acids	LRQKBLKVPFOOQJ-UHFFFAOYSA-N	CCCCC(C(=O)O)N
57	Kynurenine	Positive	[M+H]+	7.657	209.09171	209.09207	C10H12N2O3	Alkyl-phenylketones	YGPSJZOEDVAXAB-UHFFFAOYSA-N	O=C(O)CN(C(C(=O)C=1C=CC=CC1N
58	Ienticin	Positive	[M+H]+	5.584	247.14391	247.1441	C14H18N2O2	Alpha amino acids	AOHCBEAZXHZMOR-UHFFFAOYSA-N	O=C([O-])C(CC1=CNC=2C=CC=CC21)[N+](C)(C)C
59	Leucine	Positive	[M+H]+	7.598	132.1015	132.10191	C6H13NO2	L-alpha-amino acids	LRQKBLKVPFOOQJ-UHFFFAOYSA-N	CCCCC(C(=O)O)N
60	Lysine	Positive	[M+H]+	9.576	147.11259	147.11281	C6H14N2O2	D-alpha-amino acids	KDXKERNSBIXSRK-YFKPBYRVSA-N	NCCCC[C@H](N)C(O)=O
61	Melibiose	Positive	[M+Na]+	9.871	365.1055	365.10544	C12H22O11	O-glycosyl compounds	DLRVVLDZNNYCBX-ZZFZYMBESA-N	OCC1OC(OCC2OC(O)C(O)C(O)C2O)C(O)C(O)C1O
62	Methionine	Positive	[M+H]+	8.117	150.05769	150.058	C5H11NO2S	Methionine and derivatives	FFEARJCKVFRZRR-UHFFFAOYSA-N	O=C(O)C(N)CCSC
63	N-alpha-Acetyl-L-ornithine	Negative	[M-H]-	10.25	173.0925	173.09317	C7H14N2O3	N-acyl-L-alpha-amino acids	JRLGPAXAGHMNOL-LURJTMIESA-N	OC(O)=N[C@@H](CCCN)C(O)=O
64	N,N-Dimethylarginine	Positive	[M+H]+	7.969	203.14999	203.15025	C8H18N4O2	NA	NWGZOALPWZDXNG-UHFFFAOYNA-N	O=C(O)C(N(C)C)CCCNC(=N)N
65	Ornithine	Positive	[M+H]+	9.783	133.097	133.09715	C5H12N2O2	Alpha amino acids	AHLPHDHHMVZTML-UHFFFAOYSA-N	O=C(O)C(N)CCCN
66	Pantothenic acid	Negative	[M-H]-	5.872	218.1032	218.10339	C9H17NO5	Secondary alcohols	GHOKWGTUZJEAQD-ZETCQYMHSA-N	OC(C)(CO)C(=O)N[C@@H](O)C(O)=NCCC(O)=O
67	Paracetamol	Positive	[M+H]+	1.171	152.0703	152.0706	C8H9NO2	1-hydroxy-2-unsubstituted benzenoids	RZVAJINKPMORJF-UHFFFAOYSA-N	CC(O)=NC1=CC=C(O)C=C1
68	Phenethylacetate	Positive	[M+H]+	0.698	165.0903	165.091	C10H12O2	Benzene and substituted derivatives	MDHYEMXUFSJLGV-UHFFFAOYSA-N	O=C(OCCC=1C=CC=CC1)C
69	phenylacetylglutamine	Positive	[M+H]+	11.243	265.11789	265.11801	C13H16N2O4	N-acyl-alpha amino acids	JFLIEFSWGNOPJJ-JTQLQIEISA-N	O=C(O)C(N=C(O)CC=1C=CC=CC1)CC(=N)O
70	Phenylalanine	Positive	[M+H]+	7.508	166.086	166.086	C9H11NO2			O=C(O)C(N)Cc1ccccc1
71	Pipecolic acid	Positive	[M+H]+	7.212	130.08569	130.08626	C6H11NO2	Alpha amino acids	HXEACLLIILLPRG-YFKPBYRVSA-N	C1CCN(C@@H](C1)C(=O)O
72	Pipecolinic acid	Positive	[M+H]+	8.292	130.086	130.08626	C6H11NO2	Alpha amino acids	HXEACLLIILLPRG-UHFFFAOYNA-N	OC(=O)C1CCCCN1
73	Piperine	Positive	[M+H]+	0.717	286.14331	286.14377	C17H19NO3	Alkaloids and derivatives	MXXWOMGUGJBKIW-YPCIICBESA-N	O=C(\C=C\C=C\C1=CC2=C(OCO2)C=C1)N1CCCCC1
74	Proline	Positive	[M+H]+	8.208	116.0704	116.0706	C5H9NO2	Proline and derivatives	ONIBWKKTOPOVIA-UHFFFAOYNA-N	OC(=O)C1CCCN1
75	Proline-hydroxyproline	Positive	[M+H]+	10.434	229.1274	229.11829	C10H16N2O4	Dipeptides	ONPXCLZMBSJLSP-UHFFFAOYNA-N	O=C(O)C1N(C(=O)C2NCCC2)CC(O)C1
76	Pseudouridine	Negative	[M-H]-	5.752	243.0621	243.06226	C9H12N2O6	Nucleoside and nucleotide analogues	PTJWQPHWPFNBW-UHFFFAOYNA-N	OC1=NC=C(C(O)=N1)C2OC(CO)C(O)C2O
77	Pyroglutamic acid	Positive	[M+H]+	10.583	130.0497	130.0504	C5H7NO3	Amino acids	ODHCTXKNWHHXJC-UHFFFAOYNA-N	O=C(O)C1NC(=O)CC1
78	Rhynchophylline	Positive	[M+Na]+	8.377	407.18881	407.19	C22H28N2O4	Indolizidines	DAXYUDFNWXHGBE-KAXDATADSA-N	O=C(OC(=COC)C1CC2N(CCC32C(=O)NC=4C=CC=CC43)CC1CC
79	Serine	Positive	[M+H]+	10.995	106.0494	106.04987	C3H7NO3	Serine and derivatives	MTCFGRXMJLQNBG-UHFFFAOYNA-N	NC(CO)C(O)=O
80	sn-Glycero-3-phosphocholine	Positive	[M]+	10.821	258.1098	258.10956	C8H21NO6P	Glycerophosphocholines	SUHOQUVVVLNYQR-MRVPVSSYSA-O	C[N+](C)(C)CCOP(O)(=O)OC[C@H](O)CO
81	Taurine	Negative	[M-H]-	9.031	124.0071	124.00739	C2H7NO3S	Organosulfonic acids	XOAAWQZATWQOTB-UHFFFAOYSA-N	O=S(=O)(O)CCN

Table S1: Demographic Information

n	13
Age (years): Median [Range]	47 [19-64]
Gender	
Male	6 (46.2)
Female	7 (53.8)

Table S3: Microbiome Dataset Phylum and Symptoms score

	Phylum	mild_symptoms	moderate_symptoms	statistic	df	p	p.adj	p.adj.signif
1	p__Crenarchaeota	0	1	2.65023609	74.9007931	0.00981	0.04905	*
2	p__Cyanobacteria	0	1	2.78380459	48.4518919	0.00764	0.04905	*
3	p__Firmicutes	0	1	-3.0583608	55.3237504	0.00343	0.04905	*
4	p__Bacteroidetes	0	1	-2.339609	51.1879021	0.0232	0.065	ns
5	p__Chloroflexi	0	1	2.27891505	63.6827473	0.026	0.065	ns
6	p__Spirochaetes	0	1	2.42550735	44.0284889	0.0195	0.065	ns
7	p__Verrucomicrobia	0	1	1.99772006	60.1674897	0.0503	0.10778571	ns
8	p__Acidobacteria	0	1	0.93065836	73.2509802	0.355	0.52090909	ns
9	p__Actinobacteria	0	1	0.88037904	66.5237391	0.382	0.52090909	ns
10	p__Euryarchaeota	0	1	1.0100773	61.7175791	0.316	0.52090909	ns
11	p__Fusobacteria	0	1	1.03470669	44.0000997	0.306	0.52090909	ns
12	p__Lentisphaerae	0	1	-0.802856	71.5791369	0.425	0.53125	ns
13	p__Gemmatimonadetes	0	1	-0.5939425	57.3842922	0.555	0.59464286	ns
14	p__Proteobacteria	0	1	-0.6453448	50.9799637	0.522	0.59464286	ns
15	p__Tenericutes	0	1	-0.1917242	46.5644433	0.849	0.849	ns

Table S4. Metabolic Set Enrichment Analysis (MSEA) statistics comparing metabolic pathways enriched during the "acute phase" of hookworm infection, relative to baseline (i.e. "pre-infection phase")

No	Metabolic pathway	Total compounds[a]	Hits	Q-statistic	Expected Q-Statistic	Enrichment Ratio[b]	Nominal P-value	Holm P-value	FDR[c]
1	Galactose metabolism	27	1	27.77	4.35	6.388	0.0081	0.285	0.285
2	Tryptophan metabolism	41	3	12.26	4.35	2.821	0.0496	1	0.581
3	D-glutamine & D-glutamate metabolism	6	1	13.04	4.35	2.999	0.083	1	0.581
4	Glyoxylate & dicarboxylate metabolism	32	1	13.04	4.35	2.999	0.083	1	0.581
5	Nitrogen metabolism	6	3	13.04	4.35	2.999	0.083	1	0.581
6	Alanine, aspartate and glutamate metabolism	28	2	6.84	4.35	1.574	0.196	1	0.809

[a]Total number of metabolites deposited in the KEGG metabolic pathway database

[b] **Enrichment ratio:** Ratiometric enrichment expressed as acute phase/pre-infection phase

[c] P-value adjusted for False discovery rate (FDR) according to the procedure of Benjamin and Hochberg *(57)*

Table S5. Metabolic Set Enrichment Analysis (MSEA) statistics comparing metabolic pathways enriched during the "chronic phase" of hookworm infection, relative to baseline (i.e. "pre-infection phase")

No	Metabolic pathway	Total compounds[a]	Hits	Q-statistic	Expected Q-Statistic	Enrichment Ratio	Nominal P-value	Holm P-value	FDR[b]
1	Phenylalanine, tyrosine and tryptophan metabolism	4	2	8.63	4.35	1.985	0.149	1.00	0.612
2	Selenocompound metabolism	20	1	9.08	4.35	2.089	0.152	1.00	0.612
3	Ubiquinone and other terpenoid-quinone biosynthesis	9	1	7.66	4.35	1.762	0.190	1.00	0.612
4	Tyrosine metabolism	42	1	7.66	4.35	1.762	0.213	1.00	0.612
5	Phenylalanine metabolism	10	3	6.54	7.66	1.387	0.246	1.00	0.612
6	Tryptophan metabolism	41	3	6.03	7.66	1.339	0.256	1.00	0.612

[a]Total number of metabolites deposited in the KEGG metabolic pathway database

[b] **Enrichment ratio:** Ratiometric enrichment expressed as chronic phase/pre-infection phase

[c] P-value adjusted for False discovery rate (FDR) according to the procedure of Benjamin and Hochberg *(57)*

Table S6. PERMANOVA Analysis identifying "Sex" and "Participant ID" as important covariates to control for in downstream statistical analyses

Factor	Df	Sum of Squares	R^2	F	Pr(>F)
Sex	1	0.12153	0.18997	7.9168	0.001***
Participant ID	1	0.02956	0.04621	1.9257	0.072
Timepoint	1	0.00865	0.01351	0.5632	0.792
participantID:timepoint	1	0.00412	0.00645	0.2686	0.986
Residual	31	0.47589	0.74386		
Total	35	0.363975	1		

Significant codes: p < 0***, p < 0.001**, p < 0.05*

Table S7: Two-way, repeated-measures Mixed ANOVA analysis, controlling for "sex" and "participant ID" as covariates.

No	Variables	Effect	DFn	DFd	F	p	p<.05	ges	p.adj
1	Kynurenine	timepoint	2	33	5.108	0.012	*	0.236	0.5076
2	Melibiose	timepoint	2	33	4.046	0.027	*	0.197	0.5076
3	Threonic.acid	timepoint	2	33	4.089	0.026	*	0.199	0.5076
4	Indoxyl sulfate	timepoint	2	33	4.1	0.026	*	0.199	0.5076
5	Methoxypsoralen	timepoint	2	33	5.503	0.009	*	0.25	0.5076